RGG peptide induces the disassembly of disease-relevant FUS and TDP43 condensates

Mani Garg, Nayana Vinayan, Poulami Ghosh, Kesavardhana Sannula and Purusharth I Rajyaguru

Department of Biochemistry, Indian Institute of Science

Bangalore 560012

Abstract

Dynamic membraneless ribonucleoprotein (RNP) condensates regulate different processes within a cell. The assembly and disassembly of these structures are intricately regulated to maintain cellular homeostasis. Dysregulation of these structures has been implicated in various neurodegenerative disorders like Amyotrophic Lateral Sclerosis (ALS) and Frontotemporal Dementia (FTD). Identifying molecules that can disassemble these toxic assemblies is a promising approach to abrogate the associated disease phenotypes augmented by these condensates but is still poorly explored. In this study, we have identified a role for low-complexity peptide rich in arginine and glycine as a disassembly factor for mutant FUS and TDP43 condensates. Deletion of RGG-motif-containing yeast protein Sbp1 reduces the disassembly of FUS and TDP43 condensates and increases toxicity. Consistent with that, the expression of Sbp1 in human cells reduced the cytoplasmic condensates of FUS and TDP43 mutants (FUS-P525L and TDP43 lacking nuclear localization signal-ΔNLS) and increased nuclear localization of the FUS-P525L in an RGG-motif dependent manner. In accordance with the yeast data, we observed that the viability of cells expressing FUS-P525L improved upon the expression of Sbp1. *In-cell* sedimentation assay revealed that purified Sbp1 could partition FUS-P525L, but not the TDP43-ΔNLS mutant, from enriched insoluble condensates to soluble fraction. *In-vitro* sedimentation assay using a two-component purified system confirmed that partitioning of FUS, but not TDP43, increased to the soluble fraction in an RGG-motif-dependent manner. Finally, incubating the cells expressing FUS-P525L and TDP43-ΔNLS mutant with RGG-peptide resulted in a reduction of condensate size within the cells, suggesting the sufficiency of RGG peptides. Overall, our results identify a role of RGG-peptide in disassembling mutant FUS and TDP43 condensates implicated in ALS, projecting their possible therapeutic role in treating ALS.

Keywords

Neurodegenerative disorder, amyotrophic lateral sclerosis (ALS), ribonucleoprotein (RNP) condensates, condensate disassembly, intrinsically disordered region (IDR), low-complexity sequences (LCSs), RGG motif, Sbp1, FUS, FUS-P525L, TDP43, and TDP43-ΔNLS

Introduction

Cells are decorated with numerous organelles that orchestrate different kinds of functions. While membrane-bound organelles have been well studied for many years, recent reports highlight the essential role of various membraneless structures in diverse cellular processes. These dynamic and reversible structures contain several RNAs and proteins (therefore called ribonucleoprotein or RNP condensates). RNP condensates have emerged as major regulatory hubs for RNA transcription, splicing, storage, degradation, transport, and translation repression[1–8]. Stress granules (SGs) are one of the cytoplasmic RNP condensates that are formed in response to various stress conditions (like heat, osmotic, and oxidative stress)[3,9,10]. These are majorly the sites of mRNA triage where translationally stalled mRNAs are stored during stress conditions[6].

The assembly and disassembly of SGs are tightly regulated to maintain cellular homeostasis. While the formation of SGs is essential for many cellular responses[2,3,11], a timely disassembly is also necessary for maintaining cellular health. The persistent SGs are one of the characteristic features of various neurological disorders such as amyotrophic lateral sclerosis (ALS) and frontotemporal dementia (FTD)[12]. In such cases, the material properties of the SGs shift from a liquid to a more solid state, resulting in the entrapment of proteins like TDP43 and FUS, which are nuclear proteins but are observed to be mislocalized to cytoplasmic condensates often induced by specific mutations. Therefore, SGs can act as crucibles for pathological cellular assemblies, seeding the formation of toxic aggregates. The disease phenotypes could be contributed by the gain of function upon cytoplasmic condensate formation as well as upon loss of the nuclear function. A few reports have identified targets that can limit the recruitment and the associated toxicity of TDP43 and FUS to SGs in various ALS models[13–17]. However, the biomolecules that can promote the disassembly (and not clearance) of these structures are poorly explored. Notably, the sporadic nature of most ALS cases makes it challenging to identify patients before symptoms arise. Consequently, an effective therapeutic strategy would be to focus on slowing disease progression by targeting disassembly. In this direction, the identification of disassembly factors will be beneficial for these conditions where the proteins are already localized to these condensates.

Intrinsically disordered region (IDR) containing proteins have been extensively associated with the RNP condensate assembly[2,18]. Interestingly, apart from being present in abundant numbers (50%) in the proteome of SGs, around 20% of the disassembly-engaged proteins were also depicted to have IDR regions[19]. Since these proteins have the tendency to engage in several interaction networks, we hypothesized that these could have an important role to play in the disassembly of different RNP condensates. A recent report also highlights the role of an IDR-containing protein, Sbp1, from *Saccharomyces cerevisiae* in the disassembly of processing bodies (PBs, another type of cytoplasmic RNP condensate)[20]. Sbp1 is a modular protein having a central RGG/RG repeats rich RGG-motif flanked on either side by RNA-recognition motifs (RRM, Figure 1A). Apart from its role in translation repression and decapping modulation, it interacts with a core PB-residing protein, Edc3, by its low complexity RGG-motif and competes with other Edc3 molecules to disrupt the Edc3:Edc3 self-interaction[20–22]. The RGG-motif was also reported to be necessary and sufficient for the

disassembly activity, therefore establishing the role of such IDRs in the disassembly of physiological RNP condensates.

In the current report, we explore the role of the RGG-motif sequence in the disassembly of mutant TDP43 and FUS condensates. Our data from *Saccharomyces cerevisiae*, mammalian cells, *in-vitro,* and *ex-vivo* experiments propose that the RGG peptides can directly disassemble pathological condensates, raising the possibility of a therapeutic role of the RGG peptides in treating ALS.

Results

Δ*sbp1* is defective in the disassembly of TDP43, and FUS condensates

Saccharomyces cerevisiae has been widely used as a model system to understand various neurological disorders[23–29]. The overexpression of ALS-associated proteins, TDP43 and FUS, is toxic to yeast cells, and multiple reports have identified the modulators of this phenotype[23,30–36]. Overexpression can be carried out by expressing the target protein under a galactose-inducible promoter, as has been done for both TDP43 and FUS[33,37]. By using this system, we wanted to understand the role of RGG-motif-containing protein Sbp1 in the disassembly of TDP43 and FUS condensates. Yeast cells overexpressing TDP43 and FUS under a galactose-inducible promoter were incubated in galactose-containing media to induce the expression of TDP43/FUS. During this phase, the newly translated TDP43/FUS protein induces stress (termed 'induction') and accumulates in the cytoplasmic condensates (Figure 1B and E). After induction, the cells were allowed to grow in glucose-containing media. During this growth time, the protein levels will be reduced because of the inhibition of galactose promoter in glucose media. This reduction will lead to the rescue of cells from stress (termed 'recovery') and a subsequent decrease in the number of condensates. The amount of protein present in the condensates was then assessed and compared between wild-type and *Δsbp1* cells to understand the role of Sbp1 protein in the assembly and disassembly of the TDP43/FUS condensates.

The induction of TDP43 condensates was first assessed in wild-type and *Δsbp1* cells. The fraction of protein present in the condensates was comparable in both backgrounds after induction (Figure 1B and C). However, the fraction of TDP43 protein in condensates during recovery was observed to be more in the *Δsbp1* background than in the wild-type cells (Figure 1B and C). The dynamics of FUS condensates also followed a similar trend in the *Δsbp1* as compared to the wild-type background (Figure 1E and F). While the fraction of FUS protein localized to condensates was comparable between wild type and *Δsbp1*, there was a significant defect in the disassembly of protein out of condensates during recovery from stress induced by FUS overexpression (Figure 1E and F). These observations highlight the importance of Sbp1 in regulating the disassembly of TDP43 and FUS condensates in yeast cells.

One of the possible reasons for the disassembly defect in the *Δsbp1* background could be because of an increase in TDP43 and FUS levels. To understand this, the total protein levels were compared for TDP43 and FUS by Western analysis (Figure 1D and G, and Supplementary Figure 1A and B). The relative levels of protein reduction were comparable in different backgrounds for both TDP43 and FUS. Therefore, the defective disassembly could not be

attributed to TDP43 and FUS protein accumulation in the *Δsbp1* background. Overall, based on these observations, we propose a role of Sbp1 in the disassembly of TDP43 and FUS condensates in yeast cells.

TDP43 and FUS overexpression-mediated toxicity increases in *Δsbp1*

TDP43 and FUS overexpression-mediated cytotoxicity have been well-documented in yeast cells[33–35,37]. Cells transformed with a galactose-inducible *TDP43/FUS*-expressing vector show condensate formation in the cytoplasm, which leads to cytotoxicity. To further understand the role of Sbp1 in TDP43 and FUS overexpression-mediated cytotoxicity, we investigated the growth of TDP43 and FUS overexpressing cells in Δ*sbp1* background.

TDP43 and FUS overexpressing cells were significantly defective in their growth compared to the empty vector-transformed cells in both backgrounds, as observed in spot assay (Supplementary Figure 1C and D, and Figure 1H and I). *SBP1* deletion led to an aggravation of the growth defect of TDP43 overexpressing cells as compared to the wild-type cells (Figure 1H and Supplementary Figure 1C). Similarly, the deletion of *SBP1* also increased the sensitivity of cells to FUS overexpression (Figure 1I and Supplementary Figure 1D). Based on these results, we conclude that the deletion of *SBP1* sensitizes yeast cells to the overexpression of TDP43/FUS. This observation is consistent with defective condensate disassembly observed in Figure 1B and E.

Sbp1 expression reduces the mutant TDP43, and FUS condensates in mammalian cells

In order to understand the role of Sbp1 as a modulator of TDP43/FUS condensates further, we aimed to explore the effect of Sbp1 in mammalian cell models. Since there is no homolog of Sbp1 in the mammalian system, *SBP1* from *Saccharomyces cerevisiae* was cloned into mammalian expression constructs. Several disease-relevant mutants of TDP43 and FUS have been characterized. TDP43-ΔNLS (lacking nuclear localization signal, Figure 1A) mutant mislocalizes to cytoplasm and forms condensates, which are reported to be toxic and clinically relevant[38–40]. TDP43-WT was observed to be localized to the nucleus, whereas a significant number of cells with cytoplasmic condensates were observed when the TDP43-ΔNLS mutant was expressed in HEK293T cells (Figure 2A). The expression of Sbp1 led to a significant increase in the cells without condensates of the mutant protein (Figure 2A and B). Interestingly, this phenotype was significantly affected when an RGG-motif deletion mutant of Sbp1 was tested for its effect (Figure 2A and B). No change in the nuclear localization was observed for the TDP43-WT protein. Further, the Western analysis of TDP43-WT and ΔNLS mutant proteins were compared to check the role of Sbp1 or Sbp1ΔRGG in regulating their levels (Figure 2C and D). No significant change was observed for any of the proteins in the presence of Sbp1 or Sbp1ΔRGG. We conclude that Sbp1 reduces the cytoplasmic condensates of ΔNLS mutant of TDP43 in mammalian cells in an RGG-motif-dependent manner.

A similar experiment was also conducted for FUS WT and P525L mutant, where the mutation is in the NLS motif of the protein and has been correlated with an aggressive form of juvenile ALS[41] (Figure 1A). Because of this mutation, the protein mislocalizes to the cytoplasm and forms cytoplasmic condensates[42–44] (Figure 2E). HEK293T cells were co-transfected with Sbp1/Sbp1ΔRGG and FUS-WT/P525L expressing plasmids and assessed for the condensates

24 hours after transfection. As observed for TDP43 mutants, the expression of Sbp1 led to an increase in cells without FUS-P525L cytoplasmic condensates (Figure 2E and F). Similarly, the expression of the RGG deletion mutant of Sbp1 did not increase the cells without P525L condensates in a manner comparable to the wild type (Figure 2E and F). This phenotype was not due to any change in FUS protein levels, as the Western analysis reflected no significant change in FUS protein in any of the conditions (Figure 2G and H). A similar effect was observed using a different construct expressing FLAG-tagged Sbp1, which reduced cells with mutant TDP43 and FUS condensates, highlighting that the effect is not due to anomalous behavior induced by the mScarlet tag (Supplementary Figure 2A-D). Overall, we conclude that Sbp1 expression in mammalian cells significantly reduces the cytoplasmic condensates of both TDP43 and FUS mutant proteins.

Sbp1 expression reduces the defects associated with FUS-P525L overexpression in mammalian cells

Apart from inducing the reduction of cells with condensates, the effect of Sbp1 in rescuing the nuclear localization of FUS-P525L was also assessed. An analysis of the nuclear to-cytoplasm ratio of the cells expressing both FUS-P525L and Sbp1 reflected that Sbp1 expression led to an increase in the nuclear localization of the mutant FUS (Figure 3A). Moreover, the RGG-motif deletion mutant was significantly defective in rescuing the nuclear localization defect as compared to the wild type (Figure 3A). No change in the localization of FUS-WT was observed in the presence of either Sbp1 or Sbp1ΔRGG.

Overexpression of FUS has been associated with increased toxicity in HeLa cells[45]. Considering the deletion of Sbp1 aggravated the growth defects of FUS and TDP43 overexpression in yeast cells, we next explored if the expression of Sbp1 could rescue the toxicity of FUS overexpressing cells. To assess the cell viability, the number of propidium iodide-positive cells were counted in an incucyte chamber starting after 6 hours of transfection. The overexpression of FUS-WT and P525L mutant depicted increased accumulation of dead cells as compared to mock and empty vector-transfected cells (Figure 3B and C, and Supplementary Figure 3). While not significant, we also observed slightly increased toxicity of FUS-P525L in all the time points of our analysis. Although Sbp1 did not significantly affect the cell viability of eGFP-transfected cells, we observed a significant reduction in the toxicity of both FUS-WT and P525L in the presence of Sbp1 (Figure 3B and C). This result highlights the role of Sbp1 in suppressing FUS-overexpression-mediated toxicity in mammalian cells. Therefore, apart from reducing the cells with condensates, the expression of Sbp1 reduces the defects associated with the FUS-P525L in mammalian cells.

Sbp1 leads to the disassembly of FUS condensates

The reduction in the cells with condensates might result either from the defective assembly of TDP43/FUS condensates or from increased disassembly of the pre-formed condensates. Therefore, we focused on understanding the mechanism underlying the impact of Sbp1 on mutant FUS and TDP43 condensates.

In this direction, we started by assessing the disassembly activity of Sbp1 on enriched FUS condensates from HEK293T cells by using a modified *in-cell* sedimentation assay[46]. Briefly,

recombinant Sbp1 was incubated with the enriched condensates (see methods) of FUS-P525L and incubated for 1 hour at 30^0C (Figure 4A). The supernatant (soluble) and pellet (insoluble) fractions were then separated by centrifugation at 18000g for 15 minutes. If Sbp1 affects the disassembly of FUS mutant condensates, FUS protein will partition more in the supernatant (soluble) phase upon incubation with purified Sbp1 compared to the control (buffer) condition. Western analysis was carried out to check protein distribution in soluble and insoluble fractions. GAPDH, a soluble cytoplasmic protein, did not partition into the pellet fraction as expected (Figure 4B and D). On the contrary, FUS-P525L localization to the cytoplasmic condensates led to its enrichment to the insoluble pellet fraction (Figure 4B). Strikingly, the incubation of Sbp1 resulted in a significant redistribution of FUS-P525L protein to the soluble phase (Figure 4B and C). Such a phenotype was not observed for buffer control. Interestingly, when the RGG-motif deletion mutant of Sbp1 was assessed for its disassembly activity on the FUS-P525L mutant, we observed a significant defect compared to the full-length protein (Figure 4B and C). These observations suggest the RGG-dependent disassembly activity of Sbp1 on the enriched FUS-P525L condensates. Contrary to the FUS-P525L, the enriched TDP43-ΔNLS condensates failed to disassemble in the presence of Sbp1 or Sbp1ΔRGG using this assay (Figure 4D and E). Therefore, Sbp1 may act differentially on mutant TDP43, and FUS condensates inside a cell to induce their disassembly.

A simple two-component purified system-based sedimentation assay was performed to address whether Sbp1 could directly affect mutant FUS or TDP43 condensates (Figure 4F). Purified recombinant FUS or TDP43 protein was subjected to phase separation to form the condensates *in-vitro* (Supplementary Figure 4A-C). Purified Sbp1 or Sbp1ΔRGG protein was then incubated with these pre-formed condensates to assess their impact. Interestingly, upon incubation with Sbp1, there was a significant enrichment of FUS in the supernatant fraction (Figure 4G and H). Further, the fraction of FUS protein in the supernatant increased with increasing concentration of Sbp1. Such a phenotype was not observed for the control reaction, where an equal amount of BSA was incubated with the pre-formed condensates. Moreover, as observed for the *in-cell* sedimentation assay, the extent of partitioning was also significantly defective after incubation with the Sbp1ΔRGG protein (Figure 4G and H). Arginine amino acid plays an important role in protein-protein and protein-RNA interactions by participating in multiple low-affinity interactions such as pi-pi and cation-pi. To test the role of RGG-motif arginines in disassembling FUS condensates, we used a mutant (AMD, arginine methylation defective) where all the arginines within its RGG-motif were converted to alanine. This mutant, like the RGG-motif deletion mutant, was significantly defective in its disassembly activity (Supplementary Figure 4D and E), indicating an important role of the arginine residues. Surprisingly, Sbp1 failed to disassemble the *in-vitro* assembled TDP43 condensates (Figure 4I and J). Therefore, with these observations from *in-cell* and *in-vitro* sedimentation assays, we conclude that Sbp1 directly disassembles FUS condensates, and the RGG-motif is necessary for this activity. Moreover, other cellular factors likely aid the disassembly of mutant TDP43 condensates.

RGG-peptides of Sbp1 disassemble TDP43-ΔNLS and FUS-P525L condensates *in-vivo*

The observations from microscopy analysis and sedimentation assays reflected the importance of the RGG-motif of Sbp1 in disassembling FUS and TDP43 condensates. We next aimed to understand the sufficiency of RGG-motif in augmenting the disassembly of mutant TDP43 and FUS condensates *in-vivo* using live-cell microscopy analysis. The RGG-motif peptides of Sbp1 were added to the culture media of HEK293T cells expressing TDP43-ΔNLS or FUS-P525L proteins and observed by live-cell microscopy analysis (Figure 5A and B). We observed a significant reduction in the condensate size of both mutants after 30 min of peptide addition (Figures 5C and D). Notably, the condensate size was reduced further after another 30 min of incubation with Sbp1-RGG peptide (Supplementary Figure 5A and B). Such a reduction was not observed when only the vehicle (solvent control) was added to the media. These observations establish the sufficiency of Sbp1-RGG peptides in disassembling TDP43-ΔNLS or FUS-P525L condensates. Overall, our results establish the RGG-motif of Sbp1 as a disassembly-inducing peptide for ALS-relevant condensates.

Discussion

In this study, we identify the low-complexity sequence (LCS) RGG-motif to be important and sufficient for the disassembly of FUS-P525L and TDP43-ΔNLS condensates *in-vivo*. Our experiments with yeast, mammalian cells, *in-vitro* reconstituted, and *ex-vivo* systems establish the involvement of the RGG-motif in regulating the dynamics of these condensates. Our conclusion is based on the following observations: 1) *Δsbp1 yeast* cells are defective in the disassembly of TDP43 and FUS condensates, 2) TDP43 and FUS overexpression-mediated toxicity in yeast increases in *Δsbp1* cells, 3) Heterologous expression of yeast RGG-motif-containing protein Sbp1 in HEK293T cells increases the number of cells without TDP43-ΔNLS, and FUS-P525L cytoplasmic condensates in RGG-motif dependent manner, 4) Sbp1 reduces the FUS overexpression mediated toxicity in mammalian cells and rescues the nuclear localization of FUS-P525L, 5) Sbp1 directly disassembles insoluble FUS-P525L condensates thereby increasing their partitioning to the soluble fraction in RGG-motif dependent manner as observed by both modified *in-cell* and *in-vitro* sedimentation assays, and 6) RGG-peptide derived from Sbp1 disassemble TDP43-ΔNLS and FUS-P525L condensates in cells when added to the media.

Saccharomyces cerevisiae has served as a simple yet powerful model organism for understanding the molecular players of various neurological disorders, including ALS[24–29]. Overexpression of TDP43 and FUS in yeast results in cytoplasmic condensate formation and imparts toxicity to the cells[33,37]. In agreement with this, we observed TDP43 and FUS-overexpression-mediated toxicity and condensate induction in yeast cells (Figure 1). Earlier studies have utilized this system to identify molecular players of the associated cytotoxicity. Kim et al. identified multiple genes that suppress or enhance TDP43 toxicity in yeast when overexpressed[23]. Likewise, specific suppressors and enhancers of cytotoxicity for FUS have also been identified[30,36]. While many modifiers have been identified for TDP43 and FUS toxicity using yeast as a model system, no previous report has explored its potential in the identification of the disassembly factors for disease-relevant condensates. In this study, using the galactose-mediated overexpression system in yeast, we aimed to assess LCS-containing factors for their role in disassembling ALS-relevant condensates of TDP43 and FUS.

Inspired by the role of Sbp1 RGG-motif in PB disassembly[20], we hypothesized that Sbp1 could disassemble TDP43 and FUS condensates. Interestingly, TDP43 and FUS also have long stretches of LCS region, with FUS having N-terminal QGSY and an RGG-motif, and TDP43 having a long C-terminal G-rich region (Figure 1A). Our observations demonstrate a defect in the disassembly of FUS and TDP43 proteins in Δ*sbp1* cells as compared to the wild-type cells (Figure 1). Respective protein levels did not increase in Δ*sbp1* condition during the stress recovery phase, highlighting that the observed phenotype could not be mediated by a change in protein levels. Our observations with the spotting assay analysis report the enhancement of TDP43 and FUS toxicity in Δ*sbp1* cells as compared to wild-type cells (Supplementary Figure 1C and D, and Figure 1H and I). Our results are supported by the observation that overexpression of Sbp1 suppresses FUS overexpression toxicity in yeast cells[30,36]. However, these studies did not assess the underlying mechanism of regulation of toxicity by Sbp1. Importantly, our study characterizes the crucial role of the LCS of Sbp1 in disassembling ALS-related condensates, a process that was previously unexplored. No such connection has been identified for TDP43 so far. Therefore, our observations establish Sbp1 as a novel and specific regulator of mutant TDP43 and FUS condensate disassembly in yeast.

Based on our results with yeast cells, we were motivated to check the effect of Sbp1 expression on TDP43 and FUS condensates in mammalian cell models. The cytoplasmic mislocalization and aggregate formation are hallmark features of TDP43 in most ALS cases[47]. Even though present in a lesser number of ALS types, FUS mislocalization, and aggregate formation are also well reported[48]. Different mutations have been identified in both TDP43 and FUS that can enhance the rate of these defects. Overexpression of such mutant forms recapitulates the ALS-related phenotype and has been instrumental in understanding different aspects of the disease[49,50]. In our experiments, we expressed TDP43-ΔNLS and FUS-P525L mutants that mislocalized and formed cytoplasmic condensates in HEK293T cells (Figure 2). Interestingly, Sbp1 expression significantly reduced the number of cells with cytoplasmic condensates of the mutant forms of TDP43 and FUS. The RGG-deletion mutant of Sbp1 was not effective in a manner comparable to the wild type (Figure 2), suggesting an important role of the LCS in this activity. It is important to note that the RGG-deletion mutant did reduce cells with mutant condensates to a certain extent, indicating that the RRM domains could also have a role to play.

The toxic phenotype of the mutant FUS has been associated with both its cytoplasmic mislocalization and condensate formation[43,50]. Apart from a rescue of the localization of FUS-P525L to the cytoplasmic condensates, we observed a change in its localization back to the nucleus in the presence of Sbp1 (Figure 3A). This change was also dependent on the Sbp1 RGG-motif. Moreover, we observed the suppression of FUS-overexpression-mediated toxicity in the presence of Sbp1 (Figure 3B and C). Therefore, on top of rescuing the defects associated with the mutant FUS, Sbp1 significantly improves the cellular fitness of mutant FUS-overexpressing cells. These observations open an altogether new direction for exploring similar LCS-containing disassembly factors for their role in mitigating the effect of toxic condensates.

Our experiments further revealed mechanistic insights into the role of RGG-motif in modulating the cytoplasmic condensates of mutant FUS and TDP43. The modified *in-cell* and *in-vitro* sedimentation assays depicted the role of low-complexity sequence as a direct disassembly-inducing factor for the FUS-P525L condensates (Figure 4). The purified Sbp1ΔRGG mutant was as defective as the buffer/BSA control in disassembling the condensates (Figure 4). It is noteworthy that the phase separation of FUS is also dependent on its LCS, including the RGG motifs[51–53]. Therefore, it is conceivable that the RGG motif of Sbp1 interacts with RGG repeats in the FUS LCS to enable disassembly. While the disassembly activity was observed for FUS-P525L condensates, no effect could be seen on TDP43-ΔNLS condensates (Figure 4) even though ΔNLS condensates were significantly reduced in cells upon expression of Sbp1 in RGG-motif dependent manner. It is likely that the dissolution of mutant TDP43 condensates by RGG peptide is accomplished in association with certain cellular factors (proteins, RNA, metabolites, etc) that are missing in enriched condensate preparations and in the two-component sedimentation assay system. Alternatively, it is possible that the material properties differ for the enriched or *in-vitro* assembled TDP43-ΔNLS condensates such that Sbp1 cannot access the residing molecules for its disassembly activity. Understanding the molecular basis underlying the lack of sensitivity of the mutant TDP43 condensates to purified Sbp1 would be a future endeavour. A recent report identified the proteome of the insoluble TDP43 fraction from the brain tissue of TDP-43ΔNLS mice[54]. Identifying some intermediate players from this study that can be further directed to induce the disassembly of toxic TDP43 condensates will be interesting. However, the sensitivity of both FUS-P525L and TDP43-ΔNLS to RGG peptides in mammalian cells is encouraging to further explore possible therapeutic applications of RGG peptides in ALS.

Different kinds of condensate targeting molecules have been identified, and many of these primarily target the assembly of proteins into condensates[13–17]. The list includes many small molecules and a few peptides. Small planar compounds, like mitoxantrone, have been identified as affecting both the assembly and disassembly of mutant TDP43 condensates, reducing the cumulative death rate of the primary neurons[55]. Apart from these, the current literature on peptides targeting TDP43 only reports the degradation-promoting peptides[56,57]. These peptides were designed to have a TDP43 recognition motif, which is a part of the TDP43 protein having the ability to self-associate. No such peptides are reported for FUS condensates to the best of our knowledge. Our report, for the first time, identifies a peptide that functions as a genuine disassembly factor (Figure 5). Such insight has opened a new direction for exploring the role of LCS peptides as the disassembly factors of other disease-relevant RNP condensates (Figure 6). Our study provides proof of principle to explore the role of RGG-peptides as a therapeutic avenue for treating ALS. The use of treatments like ASOs and targeted degradation of aggregated proteins will have an associated drawback as they will not be able to rescue the nuclear functions of TDP43 and FUS. Rescue of the nuclear localization of FUS-P525L mutant by Sbp1 in our studies (Figure 3A) suggests that disassembly-inducing molecules could also promote nuclear relocalization. Therefore, a therapeutic option that specifically targets the disassembly of TDP43/FUS condensates could, in principle, also rescue the nuclear functions. Testing the role of RGG peptides in ALS patient-derived motor neurons for their impact on TDP43/FUS condensates will be a key step in assessing the therapeutic role

of RGG peptides. Overall, our results provide an exciting new role of low complexity sequences in the disassembly of disease-relevant condensates. These results will motivate the assessment of the potential role of other LCS in condensate disassembly and rescuing toxicity.

Materials and methods

Yeast strain and growth conditions

The yeast strains used in this study are listed in Table 1. Strains were grown at 30^0C in yeast extract-peptone (YP) medium, and cells with *FUS* and *TDP43* overexpressing plasmids were maintained in synthetic defined (SD) uracil dropout media (SD-Ura$^-$) medium supplemented with 2% raffinose. For secondary cultures, cells were diluted to OD_{600} 0.1 and grown till the mid-log phase of OD_{600} 0.4-0.5. For protein induction, the cells were shifted to 2% galactose-containing media for the mentioned time after the mid-log phase. Recovery experiments were carried out in 2% glucose-containing SD-Ura$^-$ media.

Table 1: List of yeast strains used in this study

Name	Genotype	Description	Source
yPIR1	*MATa his3Δ1 leu2Δ0 met15Δ0 ura3Δ0 ('BY4741')*	Wild type (BY4741) yeast cells	[58]
yPIR25	*MATa his3D1 leu2 ura3 his3 met15 sbp1Δ::KanMX (Δsbp1)*	Wild type *Saccharomyces cerevisiae* with *SBP1* deletion	Saccharomyces genome deletion project library

Yeast spot assays

Cells were grown till the mid-log phase in SD-Ura$^-$ media supplemented with raffinose. TDP43 and FUS induction were carried out by shifting the cells to 2% galactose-containing media for 2 and 3 hours, respectively. Post-induction cells were further processed for spotting assays. For spotting assays, cells were serially diluted from 10.0 OD_{600} to 0.001 OD_{600} and spotted on the SD-Ura$^-$ glucose and galactose-containing plates. After sufficient growth, the images were acquired, and the spot area was analyzed as described earlier in Petropavlovskiy et al. 2020[59].

Plasmids

The list of plasmids used in this study is listed in Table 2. pCEP4-*HIS-SBP1-FLAG* was constructed by amplifying *HIS-SBP1-FLAG* ORF from pPROEx-*HIS-SBP1-FLAG* construct. The primers were designed using the NEBuilder primer design tool to keep the His and Flag tags intact at the N and C-terminus, respectively, and target the amplicon to the BamHI digested pCEP4 plasmid. Positive clones were confirmed using PCR reaction, and the expression was checked by transfecting the plasmid in HEK293T cells, followed by Western blotting.

Table 2: List of plasmids used in this study

Name	Description	Source

pPIR92	pRS316 Empty vector, with *URA3* and ampicillin resistance genes	This study
pPIR74	Plasmid expressing *hFUS-YFP* under a galactose inducible promoter, with *URA3* and ampicillin resistance genes	Addgene
pPIR75	Plasmid expressing *hTDP43-GFP* under a galactose inducible promoter, with *URA3* and ampicillin resistance genes	Addgene
pPIR29	*E. coli* expression vector for Sbp1 with N-terminal His and C-terminal Flag tag, Ampicillin resistance	[22]
pPIR33	*pPIR29* with amino acid 125-167 deleted from the Sbp1-ORF; Sbp1ΔRGG	[22]
pPIR34	*pPIR29* with Sbp1R125A, R129A, R131A, R135A, R137A, R141A, R145A, R149A, R153A, R155A, R159A, R161A and R165A; Sbp1-AMD	[22]
pPIR317	pCEP4, vector with CMV promoter, hygromycin, and ampicillin resistance genes	Kind gift from Prof. K. Somasundaram, IISc
pPIR337	pCEP4-His-Sbp1-Flag, pCEP4 expressing N-terminal His and C-terminal Flag-tagged *SBP1*, CMV promoter	This study
pPIR308	peGFP-C1, the vector expressing eGFP under a CMV promoter	Kind gift from Prof. Sandeep M Eswarappa, IISc
pPIR343	peGFP-FUS-WT, the vector expressing eGFP-hFUS-WT under a CMV promoter	Kind gift from Dr. Dorothee Dormann, IMB
pPIR344	peGFP-FUS-P525L, the vector expressing eGFP-hFUS-P525L mutant under a CMV promoter	Kind gift from Dr. Dorothee Dormann, IMB
pPIR313	pDEST eGFP only, the vector expressing eGFP under a hybrid CMV and doxycycline-inducible promoter	[40]
pPIR314	pDEST TDP43-WT, pPIR313 with hTDP43 cloned upstream of eGFP	[40]
pPIR315	pDEST TDP43-ΔNLS, pPIR313 with hTDP43-ΔNLS cloned upstream of eGFP	[40]
pPIR365	pcDNA-mScarlet empty vector	Kind gift from Dr. Janin Lautenschlager
pPIR364	pcDNA-Sbp1-mScarlet	This study
pPIR373	*pPIR364* with amino acids 125-167 (from the Sbp1-ORF which starts at 22nd amino acid) deleted; Sbp1ΔRGG-mScarlet	This study
pPIR375	*E. coli* expression vector pMAL-MBP-TeV-FUS-eGFP-TeV-His	Kind gift from Dr. Dorothee Dormann, IMB[51]

pPIR376	*E. coli* expression vector pJ411/TDP-43 (TDP43-TeV-MBP-His)	Kind gift from Dr. Dorothee Dormann, IMB[17]
pPIR377	*E. coli* expression vector, expressing His-TEV in a pET-24d(+) vector	Kind gift from Dr. Dorothee Dormann, IMB[51]

Mammalian cell cultures

HEK293T and HeLa cells were maintained in Dulbecco's Modified Eagle Medium (DMEM) supplemented with 10% FBS and 1X antibacterial-antimycotic solution (complete DMEM). Media was changed every 24 hours for proper growth and split after $\geq$90% confluency. Cultures were checked for Mycoplasma contamination once every month by PCR-based method.

Transfection and preparation of mammalian cell samples for microscopy analysis

For transfection, Lipofectamine 2000 or 3000 (Thermo) was used as per the manufacturer's protocol. The cells were grown, transfected, and processed on coverslips. The samples were collected 24 hours post-transfection, and the cells were fixed with 4% formaldehyde solution for 15-20 minutes. Three washes were given with 1X PBS. For the experiment in Figure 2, the coverslips were directly mounted onto slides with Fluoromount-G containing DAPI and stored at 4^0C until imaging was done.

For the experiment in supplementary figure 2A-D, immunocytochemistry was carried out to detect Sbp1 expression. Briefly, the cells were permeabilized in 0.25% TritonX100 for 25 minutes. Blocking was done for 1.5-2 hours with a buffer containing 1% BSA and 0.3% TritonX100. This was followed by primary antibody (1:200 in blocking buffer) incubation at 4^0C overnight in a humidified chamber. Three PBST (PBS + 1% Tween) washes were given the next day, and the cells were subjected to secondary antibody (1:300 in blocking buffer) incubation for 2 hours at room temperature. Further, three PBST washes were given, and nuclei were stained with DAPI. The coverslips were mounted on slides with Fluoromount-G and stored at 4^0C until imaging was done.

For the live-cell peptide uptake assay, cells were grown and transfected on 35mm glass-bottom dishes, and the plate was directly taken for microscopy. Images were acquired at 63X objective in an incubation chamber with 5% CO_2 at 37^0C. After fixing the fields, the media was changed to a fresh one containing 5µM of the Cy5-labeled peptides (synthesized from Genscript). The imaging was done for 60 minutes, with images taken at every 15-minute interval. After 60 minutes, the cells were washed in PBS thrice and resuspended in PBS to check the uptake of Cy5-labeled peptides.

Mammalian cell viability assay

The cell viability assay was performed in the Incucyte chamber. Briefly, after 6 hours of transfections, the cell media was supplemented with 500uM propidium iodide (PI), and images were acquired every hour to score the number of PI-positive cells. The cell death

analysis was performed using the IncuCyte S3 live-cell analysis instrument (Sartorius), and the change in the number of PI-positive cells (dead cells) in different conditions was plotted in the graph.

Microscopy analysis

After the growth in respective media, yeast cells were centrifuged at 14000 rpm for 15 seconds, and pellets were resuspended in 10µl of media. A total of 5µl of the cell suspension was spotted on a coverslip for live cell imaging. The Deltavision Elite microscope system was used to acquire all the images. The system was equipped with softWoRx 3.5.1 software (Applied Precision, LLC) and an Olympus 100x, oil-immersion 1.4 NA objective. The channel's exposure time and transmittance settings were selected depending on protein expression and kept the same for all the biological replicates within an experiment. Images were captured as 512 × 512-pixel files with a CoolSnapHQ camera (Photometrics) using 1 × 1 binning for yeast. All the images were deconvolved using standard softWoRx deconvolution algorithms. ImageJ was used to analyze the data, and the granules were counted using the 'Find Maxima' tool from Fiji-ImageJ software. The images were converted to 8-bit, and the plugin was run. The prominence was set from 10-30, and the number of condensates and cells was counted.

The microscopy image acquisition for mammalian cells was performed using the Andor Dragonfly Confocal Microscope or Leica SP8 Falcon Confocal Microscope (for live cell peptide uptake experiment). HEK293T cells were imaged using 63X objective and the exposure time and transmittance were adjusted according to the protein expression levels and were kept the same for all the biological replicates within an experiment. Analysis was carried out using Fiji-ImageJ software.

Total fluorescent intensities or fraction of protein in condensates were calculated by measuring the CTCF (Corrected Total Cell Fluorescence) values for the ROI. For background subtraction, three regions from the background were selected and the intensity was calculated from all three regions. This was followed by subtraction of background from the total intensity of ROI (region of interest) using the following formula:

$$CTCF = (Area\ of\ ROI * Mean\ intensity\ of\ ROI) - (Area\ of\ background * Mean\ background\ intensity)$$

For fraction condensate intensity, the intensity of all condensates from a cell is quantitated and divided with that of the total cell intensity. For cells with no condensates in the recovery phase, the value was kept at 0.

For nuclear: cytoplasm ratio analysis, the CTCF of the nucleus and total cell was quantitated by the aforementioned method. The cytoplasm intensity was calculated by subtracting the nuclear intensity from that of the total cell intensity. This was followed by calculating the ratio of N: C intensity. To normalize the values (for cells without condensates and N: C ratio in Figures 2 and 3) for the mScarlet expression levels, the respective values were divided with

the mean CTCF mScarlet values.

Expression and purification of recombinant proteins

All the primary cultures of *E coli* expression strains were cultured in LB and were grown at 37^0C overnight in the presence of appropriate antibiotics. The individual protocols for the recombinant expression and purification of the proteins used in this study are detailed below. After purification, the elutes were dialyzed against the respective buffers, flash frozen, and stored at -80^0C as 50-100µl aliquots.

Purification of MBP-TeV-FUS-eGFP-His

MBP-TeV-FUS-eGFP-His expressing pMal plasmid was transformed into *E. coli* BL21 (DE3) Rosetta competent cells and the cells were selected on 100µg/µl ampicillin and 50 µg/µl chloramphenicol containing LB agar plates. A single colony was inoculated in LB media (containing 100µg/µl ampicillin and 50 µg/µl chloramphenicol) and was incubated overnight at 37^0C and 180rpm. A secondary culture was set up from the primary culture and was grown to a final OD_{600} of 0.8. The cultures were then subjected to a cold shock by incubating the flasks on ice for 15 minutes. This helps in the induction of chaperones that help in preventing the aggregation of FUS. Post-cold shock, the FUS protein was induced with 1mM IPTG and was incubated at 10^0C for 24 hours. Following induction, the cells were pelleted at 4200rpm at 4^0C for 15 minutes. The cell pellets were stored at -80^0C.

For the Ni-NTA purification of the His tagged FUS, the cells were first resuspended in the resuspension buffer containing 50mM NaH_2PO_4, pH 8.0, 300mM NaCl, 10mM $ZnCl_2$, 40mM imidazole,4mM beta-mercaptoethanol and 10% glycerol by vortexing. To the completely resuspended cells, a final concentration of 1mg/ml RNAase,1mg/ml lysozyme, and 1X PIC was added, followed by 30 minutes of incubation. Cells were lysed by sonication at 40% amplitude for 10 minutes with 10s on and off cycles. The lysate was centrifuged at 15000rpm for 15 minutes, and the supernatant was collected in a fresh tube. Ni-NTA resin calibrated with the resuspension buffer was added to the supernatant and was incubated for binding for 2 hours at 4^0C in a nutator. After binding, the beads were washed thrice with the wash buffer (resuspension buffer without glycerol) and eluted with 500mM imidazole. The beads were spun down at 1500rpm for 1 minute, and the elute was collected. The FUS elute obtained from the Ni-NTA purification was then subjected to binding to MBP resin, which was calibrated with the resuspension buffer overnight at 4^0C in a nutator. After binding, the MBP beads were washed twice with the resuspension buffer and were eluted using resuspension buffer with 20mM maltose. The eluted proteins were then dialyzed using a buffer containing 20mM NaH_2PO_4, pH 8.1, 150mM NaCl, 5% glycerol, 1mM EDTA, and 1mM DTT. The dialyzed protein concentrations were measured using Bradford, followed by flash freezing and storage at -80^0C[51].

Purification of TDP43-TeV-MBP-His and TeV protease

TDP43 and TeV protease were both expressed in *E coli* BL21 (DE3) Rosetta pLys competent cells grown in standard LB media. TDP43-TeV-MBP-His was induced with 0.5mM IPTG and was incubated overnight at 16^0C. The pellets were resuspended in lysis buffer containing 20mM

Tris pH 8, 1M NaCl, 10mM imidazole, 10% (v/v) glycerol, and 4mM β-mercaptoethanol and were incubated on ice for 30 minutes with 1mg/ml RNAase,1X PIC and 1mg/ml lysozyme followed by sonication. The lysate was spun down at 15000rpm for 15 minutes, and the lysate was subjected to binding to Ni-NTA beads. Post binding, the beads were washed thrice with buffer containing 40mM imidazole followed by elution using 300mM imidazole[17].

TeV protease was induced overnight (16h) with 1mM IPTG at 0.6 OD_{600} at 20^0C. The induced cell pellets were resuspended in Tris lysis buffer (50mM Tris pH8, 200mM NaCl, 20mM imidazole, 10% glycerol, and 4mM b-mercaptoethanol) and were supplemented with 1mg/ml RNAase,1mg/ml lysozyme and 1X PIC. The resuspended cells were lysed by sonication. The TeV-His in the supernatant was purified by using Ni-NTA beads and washed with the Tris lysis buffer with 1M NaCl. The TeV protease was eluted using 800mM imidazole and was dialyzed against storage buffer containing 20mM Tris pH 7.4, 150mM NaCl, 20% glycerol, and 2mM DTT[51].

Purification of His-Sbp1-Flag, His-Sbp1ΔRGG-FLAG, and His-Sbp1-AMD-Flag

Recombinant His-Sbp1-Flag, His-Sbp1ΔRGG-FLAG, and His-Sbp1-AMD-Flag transformed in *E. coli* BL21 cells were induced with 1mM IPTG for 3 hours at 37^0C. The induced cell pellet was resuspended in lysis buffer (300mM NaCl, 50mM NaH_2PO_4, 1mM DTT, 11ug/ul RNase, 1mg/ml lysozyme, 1X PIC, and 10mM Imidazole) followed by sonication. Lysate was clarified by centrifugation at 15000rpm for 15 minutes at 4^0C. Clarified lysate was incubated with equilibrated Ni-NTA resin for 2 hours at 4^0C. The beads were washed thrice with wash buffer (300mM NaCl and 50mM NaH_2PO_4) containing increasing concentrations of imidazole at each step (20, 35, and 50mM). Protein was then eluted in elution buffer (50mM NaH2PO4, 300 mM NaCl, and 500 mM Imidazole). The protein was dialyzed into dialysis buffer (10mM Tris pH 7.0, 100 mM NaCl, 10% glycerol, and 1mM dithiothreitol) overnight at 4^0C. The concentration was checked by Bradford assay, and small protein aliquots were stored at -80^0C until further usage.

In-cell sedimentation assay

HEK293T cells (from one T75 flask) transfected with the respective plasmids were collected 24 hours post-transfection. The cell lysis was carried out in RIPA buffer (50mM Tris-HCl, 1% NP-40, 150mM NaCl, 1mM EDTA, 1mM Na-orthovanadate, 1mM Na-fluoride, 1X PIC, 1mM PMSF and RNase Inhibitor) for 30 minutes at 4^0C. Cell debris was removed by a mini-spin at 1000g for 2 minutes at 4^0C. Protein concentration was estimated using Bradford, and 700-800ug of lysate was further taken to separate the soluble and insoluble phases from the lysate by centrifugation at 15000g for 15 minutes at 4^0C. The supernatant was collected as the soluble cytoplasmic fraction in a fresh tube, and the pellet was resuspended in 100ul of RIPA buffer. The disassembly reaction was set up in a fresh tube with 20ul of the pellet fraction and 5uM of the purified protein. This was allowed to incubate at 30^0C for 1 hour and then centrifugated at 15000g for 15 minutes at 4^0C to separate the soluble and the pellet fractions. The pellet was resuspended in 2% SDS buffer (2% SDS, 100mM Tris-HCl, pH 7.0) and incubated for 1 hour at 30^0C. The resulting solution after that was considered to be the insoluble fraction. All samples were heated at 100^0C for 5 minutes in 1X SDS loading dye and were taken ahead for Western analysis.

In-vitro sedimentation assay for FUS and TDP43

For the *in-vitro* sedimentation assay of FUS, the phase separation of the purified MBP-FUS-eGFP-His was induced by the cleavage of the MBP tag by the TeV protease. A 50µl phase separation mixture with 1µM FUS in a buffer containing 50mM Tris pH 8, 0.5mM EDTA, and 1mM DTT was incubated at 30^0C for 1 hour with the addition of 0.1mg/ml TeV protease[51]. Change in turbidity after 1 hour indicates phase separation. The test proteins were added at the mentioned concentration to FUS in the phase separation reaction to assess their impact on phase separation. After 1 hour of phase separation, the samples were centrifuged at 20000g for 15 minutes, and the soluble and insoluble fractions were separated. The insoluble (pellet) fraction was resuspended in 50µl buffer, and equal volumes of the two fractions were loaded onto SDS-PAGE gel. CBB staining of the SDS-PAGE gels was carried out, and the ratio of FUS in the soluble to the total protein loaded (sum of FUS in the soluble and insoluble) was calculated from the band intensities analyzed by ImageLab software. The same *in-vitro* sedimentation assay protocol was also used to assess the effect of Sbp1 on TDP43 with BSA as the negative control. The only difference in the case of TDP43 was the composition of the phase separation buffer. The MBP tag cleavage of TDP43 was carried out in a 50µl reaction mix with 1µM TDP43, HEPES buffer containing 20mM HEPES, pH 7.5, 150mM NaCl, and 1mM DTT with the addition of 20µg/µl of TeV.

Western analysis

Western analysis was conducted as per the standard protocol. Blocking was done using 5% skim milk powder in TBST. Primary antibody incubation was done overnight at 4^0C. The blots were incubated at room temperature for 1 hour for secondary antibody and were developed using the Western ECL kit in a BioRad ChemiDoc. The antibodies used in this study are anti-GFP (Biolegend, 902602), anti-Pgk1 (Abcam, Ab113687), anti-Gapdh (Cloud-clone corp., MAB932Hu23), anti-mCh (Abcam, Ab167453), anti-rabbit (Jackson ImmunoResearch Lab, 111-035-003), anti-mouse (Jackson ImmunoResearch Lab, 115-035-003), and anti-rabbit-alexafluor568 (Invitrogen, A11011).

Statistical analysis

All the analyses were conducted using the GraphPad Prism software (version 8.0.2). The significance was calculated either by unpaired/paired student t-test or 2-way ANOVA with multiple comparisons. All the figure legends include the specific details of the test used and the p-value considerations. In all the graphs, the error bars represent the standard error of the mean (SEM), and the same color points in a graph depict the data from a single experimental set.

Acknowledgment

We thank Dr. Dorothee Dormann, Dr. Janin Lautenschlager, Prof. K. Somasundaram, and Prof. Sandeep M Eswarappa for sharing various plasmids. All the members of the Rajyaguru lab are acknowledged for their constant inputs, support, and encouragement. We thank the Indian Council of Medical Research (ICMR, grant#IIRPIG-2024-01-00233), Amyotrophic Lateral Sclerosis (ALS) Association (Grant#26-SGP-761) and the Department of Biotechnology,

Government of India (DBT, grant#BT/PR51975/BMS/85/23/2024) for supporting this research; the Department of Science and Technology (DST-FIST) India, and the Indian Institute of Science (IISc) for infrastructure and other support. KS acknowledges Indian Council of Medical Research (ICMR, grant#2021-14148/CMB/ADHOC-BMS) and Department of Biotechnology (DBT, grant#BT/PR50450/MED/12/1044/2023). MG thanks CSIR-UGC and SERB-India, NV thanks PMRF, and PG appreciates GATE for the financial assistance. Flowchart or model figures were generated from adapted images provided either by Biorender or Servier Medical Art (Servier; https://smart.servier.com; licensed under a Creative Commons Attribution 4.0 Unported License).

Author contributions

Conceptualization and hypothesis—PIR and MG; Experimental design—PIR, MG, and NV; Experimentation—MG, NV, and PG; Data interpretation—PIR, MG, NV, PG, and KS; Manuscript writing (first draft)—MG, Subsequent draft review and editing—PIR and MG.

Declaration of interests

We, the authors, have submitted a provisional patent application for the use of RGG-peptides in disassembling pathological condensates.

Figure Legends

Figure 1: Δsbp1 cells are defective in the disassembly of TDP43 and FUS condensates in yeast and show enhanced toxicity. (A) Schematic representation of TDP43, FUS, and Sbp1 proteins. For Sbp1, the sequence architecture of the RGG-motif is also presented. (B) Representative images for the microscopy analysis of wild-type and Δ*sbp1* cells transformed with Gal-*TDP43-GFP* plasmid. After growing to 0.4 OD_{600}, cells were shifted to galactose-containing media for 3 hours to induce TDP43 expression (stress induction), followed by 4 hours of recovery in glucose (stress recovery). Cells were taken for microscopy analysis at both steps. White arrows mark the presence of TDP43 condensates. Scale bar=2um. (C) Graph representing the fraction of the TDP43 protein present in condensates per cell. Condensate intensities were calculated and divided by the total fluorescent intensity of the respective cell. A minimum of 50 cells per experiment were analyzed from 4 independent experiments (n=4) as performed in B. An unpaired t-test was used to calculate the significance. (D) Graph depicting the relative change in TDP43 protein levels as compared to the respective induction condition. Significance was calculated using a student-paired t-test analysis (n=8). (E) Representative images for the microscopy analysis of wild-type and Δ*sbp1* cells transformed with Gal-*FUS-YFP* plasmid. After growing to 0.4 OD_{600}, cells were shifted to galactose-containing media for 2 hours to induce FUS expression (stress induction), followed by 4 hours of recovery in glucose (stress recovery). Cells were taken for microscopy analysis at both steps. White arrows mark the presence of FUS condensates. Scale bar=5um. (F) Graph representing the fraction of the FUS protein in condensates per cell. Condensate intensities were calculated and divided by the total fluorescent intensity of the respective cell. A minimum of 50 cells per experiment were analyzed from 5 independent experiments as performed in E (n=5). An unpaired t-test was used to calculate the significance. (G) Graph depicting the relative change in FUS protein levels compared to the respective induction condition. Significance was calculated using a student-paired t-test analysis (n=5). (H and I) Quantitation of the spot area from spot assays of wild-type and Δ*sbp1* cells transformed with either Gal-*TDP43-GFP* (H) or Gal-*FUS-YFP* (I) expressing constructs as performed in Supplementary Figure 1C and D. Values were normalized with respect to their EV controls. Significance was calculated by student-paired t-test analysis (n=6 and n=10 for H and I, respectively). Error bars in all graphs represent mean $\pm$SEM, and the same color points depict the data from a single experimental set for all the graphs. *, **, ***, and **** denote p-value$\leq$0.05, $\leq$0.01, $\leq$0.001, and $\leq$0.0001, respectively.

Figure 2: Sbp1 expression reduces mutant TDP43 and FUS condensates in an RGG-motif-dependent manner in mammalian cells. (A) Microscopy images of HEK293T cells co-transfected with mScar/Sbp1-mScar/Sbp1ΔRGG-mScar and different eGFP-TDP43-related constructs. Cells were collected 24 hours after transfection and processed for microscopy analysis. The white arrow marks the presence of cytoplasmic condensates. Scale bar=5um. (B) Graph representing the relative changes in the cells without TDP43-ΔNLS condensates (relative to the mScar transfected cells). The values were also normalized with the respective mScarlet fluorescent intensity expression levels. A paired t-test was used to calculate the significance value (n=6). (C and D) Western blot analysis (C) and its quantitation (D) representing the change in the levels of TDP43-WT and TDP43-ΔNLS in the presence of mScar/Sbp1-mScar/Sbp1ΔRGG-mScar from 6 independent experiments (n=6). Anti-mCh

antibody was used to detect the mScarlet-tagged proteins. Values on the right represent the position of different molecular weight ladder bands in kDa. A student-paired t-test was used to calculate the significance value. (E) Microscopy images of HEK293T cells co-transfected with mScar/Sbp1-mScar/Sbp1ΔRGG-mScar and eGFP-FUS-WT/P525L constructs. Cells were processed similarly to the experiment in A. The white arrow marks the presence of cytoplasmic condensates. Scale bar=5um. (F) Graph representing the relative changes in the cells without TDP43-ΔNLS condensates (relative to the mScar transfected cells). The values were also normalized with the respective mScarlet fluorescent intensity expression levels. A paired t-test was used to calculate the significance value (n=5). (G and H) Western blot analysis (G) and its quantitation (H) representing the change in the levels of FUS-WT and FUS-P525L in the presence of mScar/Sbp1-mScar/Sbp1ΔRGG-mScar (n=4). Anti-mCh antibody was used to detect the mScarlet-tagged proteins. Values on the right represent the position of different molecular weight ladder bands in kDa. A student-paired t-test was used to calculate the significance value. Error bars in all graphs represent mean ±SEM, and the same color points in a graph depict the data from a single experimental set. *, **, ***, and **** denote p-value≤0.05, ≤0.01, ≤0.001, and ≤0.0001, respectively.

Figure 3: Sbp1 expression reduces overexpression-mediated defects of FUS-P525L in mammalian cells. (A) Graph representing the distribution of FUS-P525L protein in nucleus and cytoplasm. The fluorescent intensities of the nucleus and cytoplasm were calculated from the experiment as performed in Figure 2E, and the ratio is plotted here. A student-paired t-test was used to calculate the significance value (n=6). (B) Incucyte images (real-time cell death analysis) representing the cellular uptake of propidium iodide (PI) in different conditions in HeLa cells. Scale bar=100um. (C) Graph representing the number of propidium iodide (PI) positive cells (dead cells) from the experiment as performed in B. The time on the x-axis reflects the time-point after transfection in hours. The significance was calculated using 2-way ANOVA with multiple comparisons (n=4). Error bars in all graphs represent mean ±SEM, and the same color points in A depict the data from a single experimental set. *, **, ***, and **** denote p-value≤0.05, ≤0.01, ≤0.001, and ≤0.0001, respectively.

Figure 4: Sbp1, but not Sbp1ΔRGG, disassembles FUS condensates. (A) Schematic depicting the workflow for the *in-cell* sedimentation assay modified to assess the disassembly activity of Sbp1. (B and D) Western analysis of the different fractions from FUS-P525L (B), and TDP43-ΔNLS (D) *in-cell* sedimentation assay. The different fraction loadings are as follows: lysate: 7.5%, cytoplasm: 7.5%, pellet: 15%, soluble: 60%, and insoluble: 60%. GAPDH serves as the control for the assay, and ponceau reflects the purified protein added to the respective reaction. Values on the right represent the position of different molecular weight ladder bands in kDa. (C and E) Quantitation of the amount of protein in the soluble fraction from experiments as done in B and D. The band intensities were calculated using ImageJ, and the fraction of protein in the soluble phase was calculated by S/(S+I), where S and I represent the protein in the soluble and the insoluble fractions, respectively. Significance was calculated by using student-paired t-test analysis (n=6 and n=7 for C and E, respectively). (F) Schematic depicting the workflow of the *in-vitro* sedimentation assay performed to assess the disassembly activity of Sbp1 on the phase-separated FUS and TDP43 condensates. (G) Coomassie-stained protein gels depicting the fractionation of FUS to soluble and insoluble

phases in the presence of buffer, BSA, Sbp1, Sbp1ΔRGG. The ratio reflects the amount of FUS: test protein taken for the assay. Sbp1ΔRGG and MBP migrate at the same position and hence appear as a single band. Values on the left represent the position of different molecular weight ladder bands in kDa. (H) Quantitation of the fraction of FUS protein present in the soluble phase from 7 independent experiments (n=7) as performed in G. Significance was calculated by a student-paired t-test analysis. (I) Coomassie-stained protein gels and its quantitation (J) depicting the fractionation of TDP43 to soluble and insoluble phases in the presence of BSA and Sbp1. The ratio reflects the amount of TDP43:test protein taken for the assay. The values on the graph reflect the relative amount of TDP43 protein present in the insoluble fraction. A student-paired t-test analysis calculated significance (n=3). Error bars represent mean ±SEM, and the same color points depict the data from a single experimental set. *, **, ***, and **** denote p-value ≤0.05, ≤0.01, ≤0.001, and ≤0.0001, respectively.

Figure 5: Sbp1-RGG peptide disassembles the TDP43-ΔNLS and FUS-P525L condensates. (A) Schematic depicting the workflow of the live-cell microscopy with the RGG-peptides. (B) The sequence of the peptide used for the experiment as performed in A. 2 extra amino acids at the N-terminal end (M and Q) and 3 amino acids at the C-terminal end (F, N, and G) were included for better purification of the RGG-peptide. (C) Microscopy images for HEK293T cells depicting the change in the area of TDP43-ΔNLS condensate (marked by white arrows) after incubating with either the vehicle control or Sbp1-RGG peptides. Scale bar=2um. Graphs on the right depict the quantitation of the condensate area/total cell area from at least 30 cells per experiment (n=3). (D) Microscopy images for HEK293T cells depicting the change in the area of FUS-P525L condensate (marked by white arrows) after incubating with either the vehicle control or Sbp1-RGG peptides. Scale bar=2um. Graphs on the right depict the quantitation of the condensate area/total cell area from at least 40 cells per experiment (n=3). Significance was calculated by paired t-test analysis. **** denotes p-value ≤0.0001.

Figure 6: Schematic depicting the role of RGG peptides as a therapeutic approach to disassemble the toxic cytoplasmic condensates. Green represents mutant proteins, like FUS-P525L and TDP43-ΔNLS, that mislocalize to the cytoplasm and form condensates in diseased conditions. RGG peptides could have the potential to disassemble these toxic condensates. Such an effect may also result in the restoration of the nuclear localization phenotype.

Supplemental Information

Supplementary Figures S1-S5.

Supplementary Figure S1: Δsbp1 cells are defective in the disassembly of TDP43 and FUS condensates in yeast. (A and B) Western analysis depicting the change in protein levels of TDP43 (A) and FUS (B) with respect to the respective induction condition. Quantitation of the blots is provided as Figure 1D and G. Values on the right represent the position of different molecular weight ladder bands in kDa. Ponceau served as the loading control. (C and D) Spot assays of wild type and Δ*sbp1* cells transformed with either empty vector (EV) or Gal-*TDP43-GFP* (C) / Gal-*FUS-YFP* (D) expressing constructs. After growing to 0.4 OD_{600}, cells were shifted to galactose-containing media for 2-3 hours to induce TDP43/*FUS* expression. This was followed by serial dilution of cells and spotting on glucose and galactose-containing SD-Ura^- media plates. Images were taken after 2 -4 days of growth at 30^0C.

Supplementary Figure S2: Sbp1 expression reduces mutant TDP43 and FUS condensates in HEK293T cells. (A) Microscopy images of HEK293T cells co-transfected with EV/Sbp1 and different eGFP-TDP43-related constructs. Cells were collected 24 hours after transfection and processed for immuno-cytochemistry analysis to detect Sbp1 using an anti-Sbp1 antibody (RFP channel). TDP43 constructs have an N-terminal eGFP-tag that was used to check the localization through the GFP channel. The white arrow marks the presence of cytoplasmic condensates. Scale bar=5um. (B) Quantitation of the percentage of cells without cytoplasmic condensates from the experiment as performed in A. A student-paired t-test was used to calculate the significance value (n=4). (C) Microscopy images of HEK293T cells co-transfected with EV/Sbp1 and eGFP-FUS-WT/P525L constructs. Cells were collected 24 hours after transfection and processed like the experiment in A. The white arrow marks the presence of cytoplasmic condensates. Scale bar=5um. (D) Quantitation of the percentage of cells without cytoplasmic condensates from the experiment as performed in C. A student-paired t-test was used to calculate the significance value (n=5). Error bars in all the graphs represent mean $\pm$SEM, and the same color points in a graph depict the data from a single experimental set. ** and **** denote p-value $\leq$0.01 and $\leq$0.0001, respectively.

Supplementary Figure S3: Sbp1 expression reduces overexpression-mediated defects of FUS-P525L in mammalian cells. Incucyte images representing the cellular uptake of propidium iodide (PI) in different conditions in HeLa cells. Scale bar=100um. The images are part of Figures 3B and C.

Supplementary Figure S4: Sbp1AMD (arginine methylation defective) mutant does not affect FUS condensates. (A) Coomassie-stained protein gel depicting the various purified proteins used in this study. (B and C) Coomassie-stained protein gels depicting the partitioning of FUS (B) and TDP43 (C) to the insoluble (I) phase after the cleavage of MBP-tag using TeV protease. S denotes the soluble phase. Values on the right represent the position of different molecular weight ladder bands in kDa. (D) Coomassie-stained protein gel depicting the fractionation of FUS to soluble and insoluble phases in the presence of Sbp1AMD (mutant where all arginines within the RGG-motif are covered to alanine, see Figure 1A). The ratio reflects the amount of FUS: test protein taken for the assay. Sbp1AMD and MBP migrate at

the same position and hence appear as a single band. Values on the left represent the position of different molecular weight ladder bands in kDa. (E) Quantitation of the fraction of FUS protein present in the soluble phase from 7 independent experiments (n=7) as performed in D and Figure 3H. The graph from Figure 3I has been replotted here to include Sbp1AMD values. Error bars represent mean ±SEM, and the same color points in a graph depict the data from a single experimental set. *, **, ***, and **** denote p-value ≤0.05, ≤0.01, ≤0.001, and ≤0.0001, respectively.

Supplementary Figure S5: HEK293T cells readily uptake Cy5-labelled Sbp1-RGG peptide. (A and B) Microscopy images for HEK293T cells depicting the change in the area of TDP43-ΔNLS (A) and FUS-P525L (B) condensate (marked by white arrows) and the uptake of Cy5-labelled peptide after 60mins of incubation with either the vehicle control or Sbp1-RGG peptides. The panel represents the same set of cells as depicted in Figure 4D. Cy5 panel depicts the uptake of the peptide. Scale bar=2um. The graph on the right represents the change in the condensate area normalized with the total cell area after incubation with the Sbp1-RGG peptide (n=3). The data plotted is the same as Figure 4D with the addition of a 60 mins time point. Error bars represent mean ±SEM. Significance was calculated by paired t-test analysis. **** denotes p-value ≤0.0001.

References

1. Lee, J., Cho, H. & Kwon, I. Phase separation of low-complexity domains in cellular function and disease. *Exp Mol Med* **54**, 1412–1422 (2022).

2. Protter, D. S. W. & Parker, R. Principles and Properties of Stress Granules. *Trends Cell Biol* **26**, 668–679 (2016).

3. Anderson, P. & Kedersha, N. Stress granules: the Tao of RNA triage. *Trends Biochem Sci* **33**, 141–150 (2008).

4. Youn, J.-Y. *et al.* Properties of Stress Granule and P-Body Proteomes. *Mol Cell* **76**, 286–294 (2019).

5. Buchan, J. R. & Parker, R. Eukaryotic Stress Granules: The Ins and Outs of Translation. *Mol Cell* **36**, 932–941 (2009).

6. Riggs, C. L., Kedersha, N., Ivanov, P. & Anderson, P. Mammalian stress granules and P bodies at a glance. *J Cell Sci* **133**, (2020).

7. Luo, Y., Na, Z. & Slavoff, S. A. P-Bodies: Composition, Properties, and Functions. *Biochemistry* **57**, 2424–2431 (2018).

8. Kiebler, M. A. & Bassell, G. J. Neuronal RNA Granules: Movers and Makers. *Neuron* **51**, 685–690 (2006).

9. Buchan, J. R., Yoon, J.-H. & Parker, R. Stress-specific composition, assembly and kinetics of stress granules in *Saccharomyces cerevisiae*. *J Cell Sci* **124**, 228–239 (2011).

10. Aulas, A. *et al.* Stress-specific differences in assembly and composition of stress granules and related foci. *J Cell Sci* (2017) doi:10.1242/jcs.199240.

11. Mahboubi, H. & Stochaj, U. Cytoplasmic stress granules: Dynamic modulators of cell signaling and disease. *Biochimica et Biophysica Acta (BBA) - Molecular Basis of Disease* **1863**, 884–895 (2017).

12. Wolozin, B. & Ivanov, P. Stress granules and neurodegeneration. *Nat Rev Neurosci* **20**, 649–666 (2019).

13. Duan, Y. *et al.* PARylation regulates stress granule dynamics, phase separation, and neurotoxicity of disease-related RNA-binding proteins. *Cell Res* **29**, 233–247 (2019).

14. McGurk, L. *et al.* Poly(ADP-Ribose) Prevents Pathological Phase Separation of TDP-43 by Promoting Liquid Demixing and Stress Granule Localization. *Mol Cell* **71**, 703-717.e9 (2018).

15. Wang, F., Li, J., Fan, S., Jin, Z. & Huang, C. Targeting stress granules: A novel therapeutic strategy for human diseases. *Pharmacol Res* **161**, 105143 (2020).

16. Becker, L. A. *et al.* Therapeutic reduction of ataxin-2 extends lifespan and reduces pathology in TDP-43 mice. *Nature* **544**, 367–371 (2017).

17. Gruijs da Silva, L. A. *et al.* Disease-linked TDP-43 hyperphosphorylation suppresses TDP-43 condensation and aggregation. *EMBO J* **41**, e108443 (2022).

18. Kedersha, N., Ivanov, P. & Anderson, P. Stress granules and cell signaling: more than just a passing phase? *Trends Biochem Sci* **38**, 494–506 (2013).

19. Marmor-Kollet, H. *et al.* Spatiotemporal Proteomic Analysis of Stress Granule Disassembly Using APEX Reveals Regulation by SUMOylation and Links to ALS Pathogenesis. *Mol Cell* **80**, 876-891.e6 (2020).

20. Roy, R., Das, G., Kuttanda, I. A., Bhatter, N. & Rajyaguru, P. I. Low complexity RGG-motif sequence is required for Processing body (P-body) disassembly. *Nat Commun* **13**, 2077 (2022).

21. Segal, S. P., Dunckley, T. & Parker, R. Sbp1p Affects Translational Repression and Decapping in *Saccharomyces cerevisiae*. *Mol Cell Biol* **26**, 5120–5130 (2006).

22. Bhatter, N. *et al.* Arginine methylation augments Sbp1 function in translation repression and decapping. *FEBS J* **286**, 4693–4708 (2019).

23. Kim, H.-J. *et al.* Therapeutic modulation of eIF2α phosphorylation rescues TDP-43 toxicity in amyotrophic lateral sclerosis disease models. *Nat Genet* **46**, 152–60 (2014).

24. Muchowski, P. J. *et al.* Hsp70 and hsp40 chaperones can inhibit self-assembly of polyglutamine proteins into amyloid-like fibrils. *Proc Natl Acad Sci U S A* **97**, 7841–6 (2000).

25. Krobitsch, S. & Lindquist, S. Aggregation of huntingtin in yeast varies with the length of the polyglutamine expansion and the expression of chaperone proteins. *Proc Natl Acad Sci U S A* **97**, 1589–94 (2000).

26. Gitler, A. D. *et al.* The Parkinson's disease protein alpha-synuclein disrupts cellular Rab homeostasis. *Proc Natl Acad Sci U S A* **105**, 145–50 (2008).

27. Cooper, A. A. *et al.* Alpha-synuclein blocks ER-Golgi traffic and Rab1 rescues neuron loss in Parkinson's models. *Science* **313**, 324–8 (2006).

28. Outeiro, T. F. & Lindquist, S. Yeast cells provide insight into alpha-synuclein biology and pathobiology. *Science* **302**, 1772–5 (2003).

29. Kryndushkin, D., Ihrke, G., Piermartiri, T. C. & Shewmaker, F. A yeast model of optineurin proteinopathy reveals a unique aggregation pattern associated with cellular toxicity. *Mol Microbiol* **86**, 1531–47 (2012).

30. Sun, Z. *et al.* Molecular Determinants and Genetic Modifiers of Aggregation and Toxicity for the ALS Disease Protein FUS/TLS. *PLoS Biol* **9**, e1000614 (2011).

31. Peggion, C. *et al.* Nucleolin Rescues TDP-43 Toxicity in Yeast and Human Cell Models. *Front Cell Neurosci* **15**, 625665 (2021).

32. Park, S.-K., Park, S. & Liebman, S. W. TDP-43 Toxicity in Yeast Is Associated with a Reduction in Autophagy, and Deletions of TIP41 and PBP1 Counteract These Effects. *Viruses* **14**, (2022).

33. Armakola, M., Hart, M. P. & Gitler, A. D. TDP-43 toxicity in yeast. *Methods* **53**, 238–45 (2011).

34. Johnson, B. S., McCaffery, J. M., Lindquist, S. & Gitler, A. D. A yeast TDP-43 proteinopathy model: Exploring the molecular determinants of TDP-43 aggregation and cellular toxicity. *Proceedings of the National Academy of Sciences* **105**, 6439–6444 (2008).

35. Fushimi, K. *et al.* Expression of human FUS/TLS in yeast leads to protein aggregation and cytotoxicity, recapitulating key features of FUS proteinopathy. *Protein Cell* **2**, 141–9 (2011).

36. Hayden, E. *et al.* A Genetic Screen for Human Genes Suppressing FUS Induced Toxicity in Yeast. *G3 (Bethesda)* **10**, 1843–1852 (2020).

37. Ju, S. *et al.* A yeast model of FUS/TLS-dependent cytotoxicity. *PLoS Biol* **9**, e1001052 (2011).

38. Chen, Y. & Cohen, T. J. Aggregation of the nucleic acid–binding protein TDP-43 occurs via distinct routes that are coordinated with stress granule formation. *Journal of Biological Chemistry* **294**, 3696–3706 (2019).

39. Voigt, A. *et al.* TDP-43-Mediated Neuron Loss In Vivo Requires RNA-Binding Activity. *PLoS One* **5**, e12247 (2010).

40. Scotter, E. L. *et al.* Differential roles of the ubiquitin proteasome system (UPS) and autophagy in the clearance of soluble and aggregated TDP-43 species. *J Cell Sci* (2014) doi:10.1242/jcs.140087.

41. Zhou, B. *et al.* FUS P525L mutation causing amyotrophic lateral sclerosis and movement disorders. *Brain Behav* **10**, e01625 (2020).

42. Chen, Y. *et al.* PINK1 and Parkin are genetic modifiers for FUS-induced neurodegeneration. *Hum Mol Genet* ddw310 (2016) doi:10.1093/hmg/ddw310.

43. Lenzi, J. *et al.* ALS mutant FUS proteins are recruited into stress granules in induced Pluripotent Stem Cells (iPSCs) derived motoneurons. *Dis Model Mech* (2015) doi:10.1242/dmm.020099.

44. Deng, J. *et al.* FUS Interacts with HSP60 to Promote Mitochondrial Damage. *PLoS Genet* **11**, e1005357 (2015).

45. Reber, S. *et al.* The phase separation-dependent FUS interactome reveals nuclear and cytoplasmic function of liquid-liquid phase separation. *Nucleic Acids Res* **49**, 7713–7731 (2021).

46. Gruijs da Silva, L. A. & Dormann, D. Sedimentation Assays to Assess the Impact of Posttranslational Modifications on Phase Separation of RNA-Binding Proteins In Vitro and In Cells. *Methods Mol Biol* **2563**, 325–339 (2023).

47. Scotter, E. L., Chen, H.-J. & Shaw, C. E. TDP-43 Proteinopathy and ALS: Insights into Disease Mechanisms and Therapeutic Targets. *Neurotherapeutics* **12**, 352–63 (2015).

48. Nolan, M., Talbot, K. & Ansorge, O. Pathogenesis of FUS-associated ALS and FTD: insights from rodent models. *Acta Neuropathol Commun* **4**, 99 (2016).

49. Lagier-Tourenne, C. & Cleveland, D. W. Rethinking ALS: the FUS about TDP-43. *Cell* **136**, 1001–4 (2009).

50. Da Cruz, S. & Cleveland, D. W. Understanding the role of TDP-43 and FUS/TLS in ALS and beyond. *Curr Opin Neurobiol* **21**, 904–19 (2011).

51. Hofweber, M. *et al.* Phase Separation of FUS Is Suppressed by Its Nuclear Import Receptor and Arginine Methylation. *Cell* **173**, 706-719.e13 (2018).

52. Bentmann, E. *et al.* Requirements for stress granule recruitment of fused in sarcoma (FUS) and TAR DNA-binding protein of 43 kDa (TDP-43). *J Biol Chem* **287**, 23079–94 (2012).

53. Portz, B., Lee, B. L. & Shorter, J. FUS and TDP-43 Phases in Health and Disease. *Trends Biochem Sci* **46**, 550–563 (2021).

54. Dunlop, F., Mason, S., Tsitkanou, S. & Russell, A. P. Proteomic analysis of the TDP-43-associated insoluble fraction from NEFH-TDP-43 mouse brain suggests sustained stress granule formation, CLUH granule recruitment and impaired mitochondrial metabolism. Preprint at https://doi.org/10.1101/2024.05.23.595607 (2024).

55. Fang, M. Y. *et al.* Small-Molecule Modulation of TDP-43 Recruitment to Stress Granules Prevents Persistent TDP-43 Accumulation in ALS/FTD. *Neuron* **103**, 802-819.e11 (2019).

56. Gao, N. *et al.* TDP-43 specific reduction induced by Di-hydrophobic tags conjugated peptides. *Bioorg Chem* **84**, 254–259 (2019).

57. Liu, R. *et al.* Reducing TDP-43 aggregation does not prevent its cytotoxicity. *Acta Neuropathol Commun* **1**, 49 (2013).

58. Poornima, G., Shah, S., Vignesh, V., Parker, R. & Rajyaguru, P. I. Arginine methylation promotes translation repression activity of eIF4G-binding protein, Scd6. *Nucleic Acids Res* gkw762 (2016) doi:10.1093/nar/gkw762.

59. Petropavlovskiy, A. A., Tauro, M. G., Lajoie, P. & Duennwald, M. L. A Quantitative Imaging-Based Protocol for Yeast Growth and Survival on Agar Plates. *STAR Protoc* **1**, 100182 (2020).

Figure 1

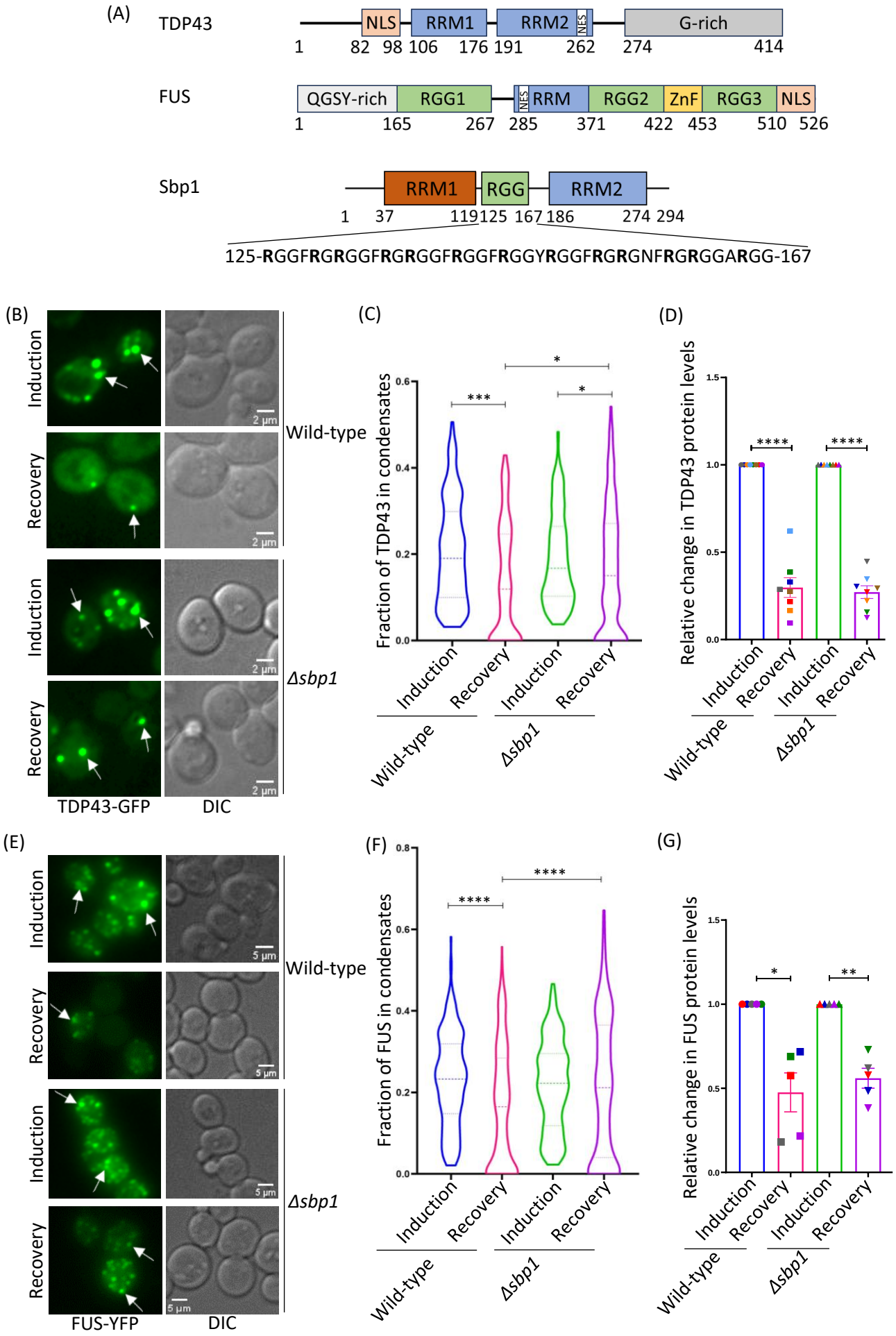
(A)
TDP43
NLS
RRM1
RRM2
NES
G-rich
1 82 98 106 176 191 262 274 414
FUS
QGSY-rich
RGG1
NES
RRM
RGG2
ZnF
RGG3
NLS
1 165 267 285 371 422 453 510 526
Sbp1
RRM1
RGG
RRM2
1 37 119 125 167 186 274 294
125-RGGFRGRGGFRGRGGFRGGFRGGYRGGFRGRGNFRGRGGARGG-167
(B)
Induction
Recovery
Wild-type
Δsbp1
TDP43-GFP
DIC
2 µm
(C)
Fraction of TDP43 in condensates
***
*
*
Induction
Recovery
Wild-type
Δsbp1
(D)
Relative change in TDP43 protein levels
****
****
(E)
FUS-YFP
5 µm
(F)
Fraction of FUS in condensates
****
****
(G)
Relative change in FUS protein levels
*
**

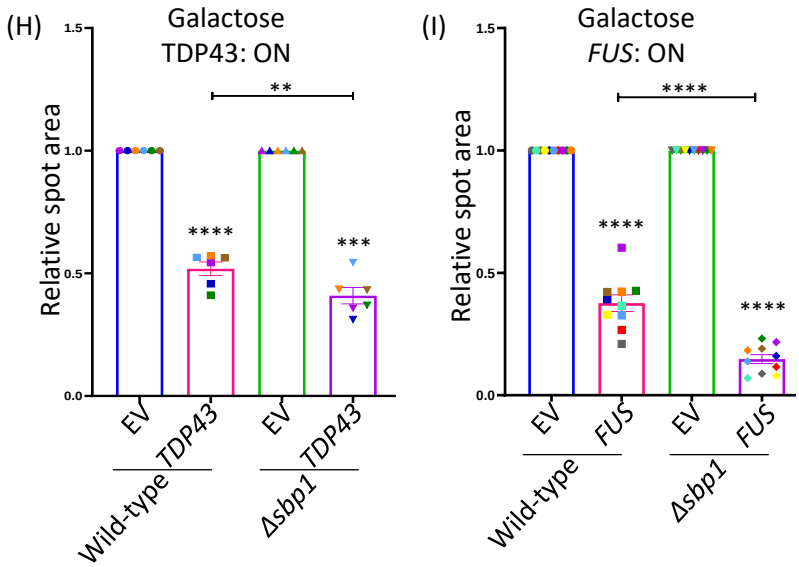

Figure 1: Δsbp1 cells are defective in the disassembly of TDP43 and FUS condensates in yeast and show enhanced toxicity. (A) Schematic representation of TDP43, FUS, and Sbp1 proteins. For Sbp1, the sequence architecture of the RGG-motif is also presented. (B) Representative images for the microscopy analysis of wild-type and Δ*sbp1* cells transformed with Gal-*TDP43-GFP* plasmid. After growing to 0.4 OD_{600}, cells were shifted to galactose-containing media for 3 hours to induce TDP43 expression (stress induction), followed by 4 hours of recovery in glucose (stress recovery). Cells were taken for microscopy analysis at both steps. White arrows mark the presence of TDP43 condensates. Scale bar=2um. (C) Graph representing the fraction of the TDP43 protein present in condensates per cell. Condensate intensities were calculated and divided by the total fluorescent intensity of the respective cell. A minimum of 50 cells per experiment were analyzed from 4 independent experiments (n=4) as performed in B. An unpaired t-test was used to calculate the significance. (D) Graph depicting the relative change in TDP43 protein levels as compared to the respective induction condition. Significance was calculated using a student-paired t-test analysis (n=8). (E) Representative images for the microscopy analysis of wild-type and Δ*sbp1* cells transformed with Gal-*FUS-YFP* plasmid. After growing to 0.4 OD_{600}, cells were shifted to galactose-containing media for 2 hours to induce FUS expression (stress induction), followed by 4 hours of recovery in glucose (stress recovery). Cells were taken for microscopy analysis at both steps. White arrows mark the presence of FUS condensates. Scale bar=5um. (F) Graph representing the fraction of the FUS protein in condensates per cell. Condensate intensities were calculated and divided by the total fluorescent intensity of the respective cell. A minimum of 50 cells per experiment were analyzed from 5 independent experiments as performed in E (n=5). An unpaired t-test was used to calculate the significance. (G) Graph depicting the relative change in FUS protein levels compared to the respective induction condition. Significance was calculated using a student-paired t-test analysis (n=5). (H and I) Quantitation of the spot area from spot assays of wild-type and Δ*sbp1* cells transformed with either Gal-*TDP43-GFP* (H) or Gal-*FUS-YFP* (I) expressing constructs as performed in Supplementary Figure 1C and D. Values were normalized with respect to their EV controls. Significance was calculated by student-paired t-test analysis (n=6 and n=10 for H and I, respectively). Error bars in all graphs represent mean ±SEM, and the same color points depict the data from a single experimental set for all the graphs. *, **, ***, and **** denote p-value≤0.05, ≤0.01, ≤0.001, and ≤0.0001, respectively.

Figure 2

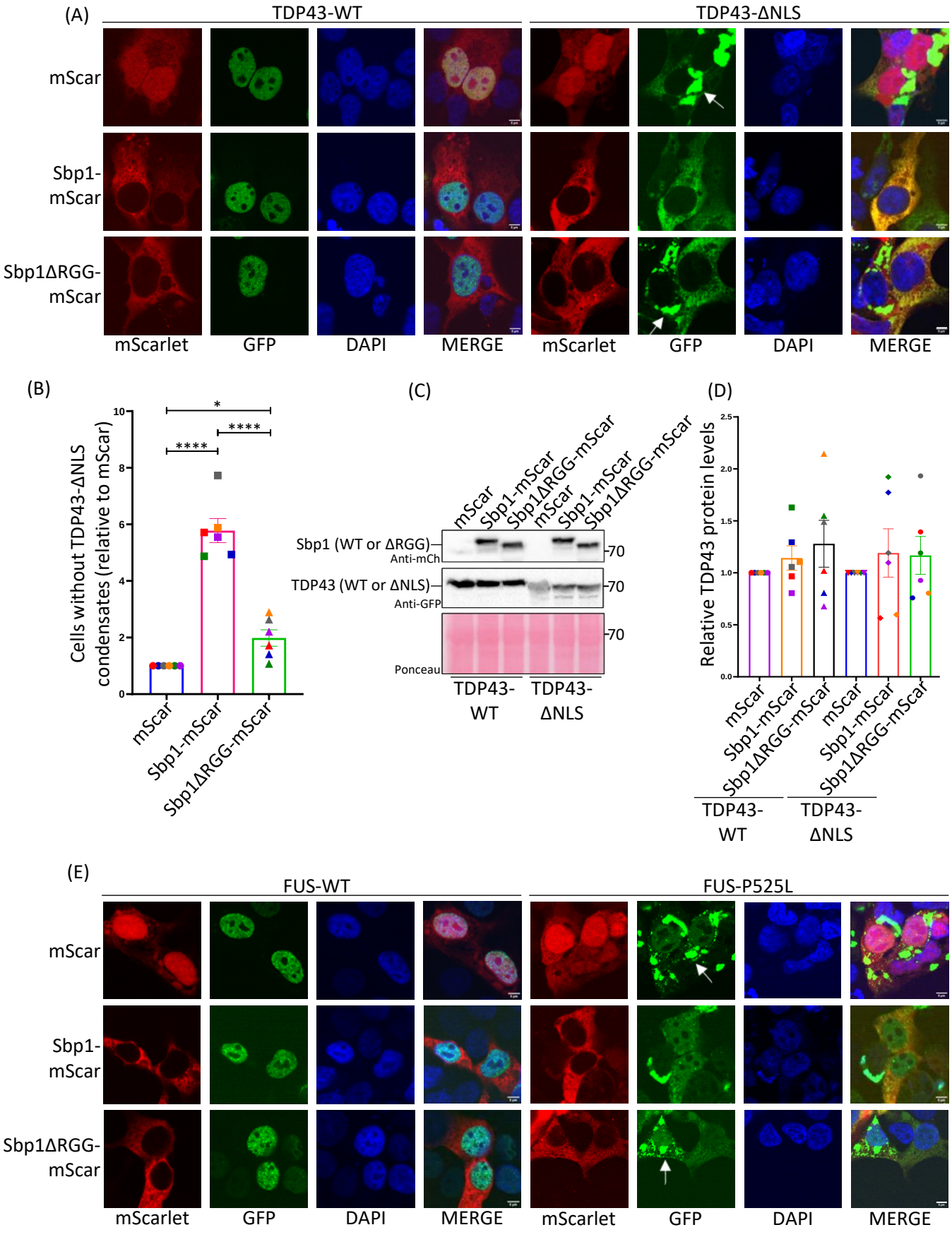
(A)
TDP43-WT
TDP43-ΔNLS
mScar
Sbp1-mScar
Sbp1ΔRGG-mScar
mScarlet
GFP
DAPI
MERGE
(B)
Cells without TDP43-ΔNLS condensates (relative to mScar)
*
****
****
mScar
Sbp1-mScar
Sbp1ΔRGG-mScar
(C)
Sbp1 (WT or ΔRGG)
Anti-mCh
TDP43 (WT or ΔNLS)
Anti-GFP
Ponceau
70
TDP43-WT
TDP43-ΔNLS
(D)
Relative TDP43 protein levels
(E)
FUS-WT
FUS-P525L

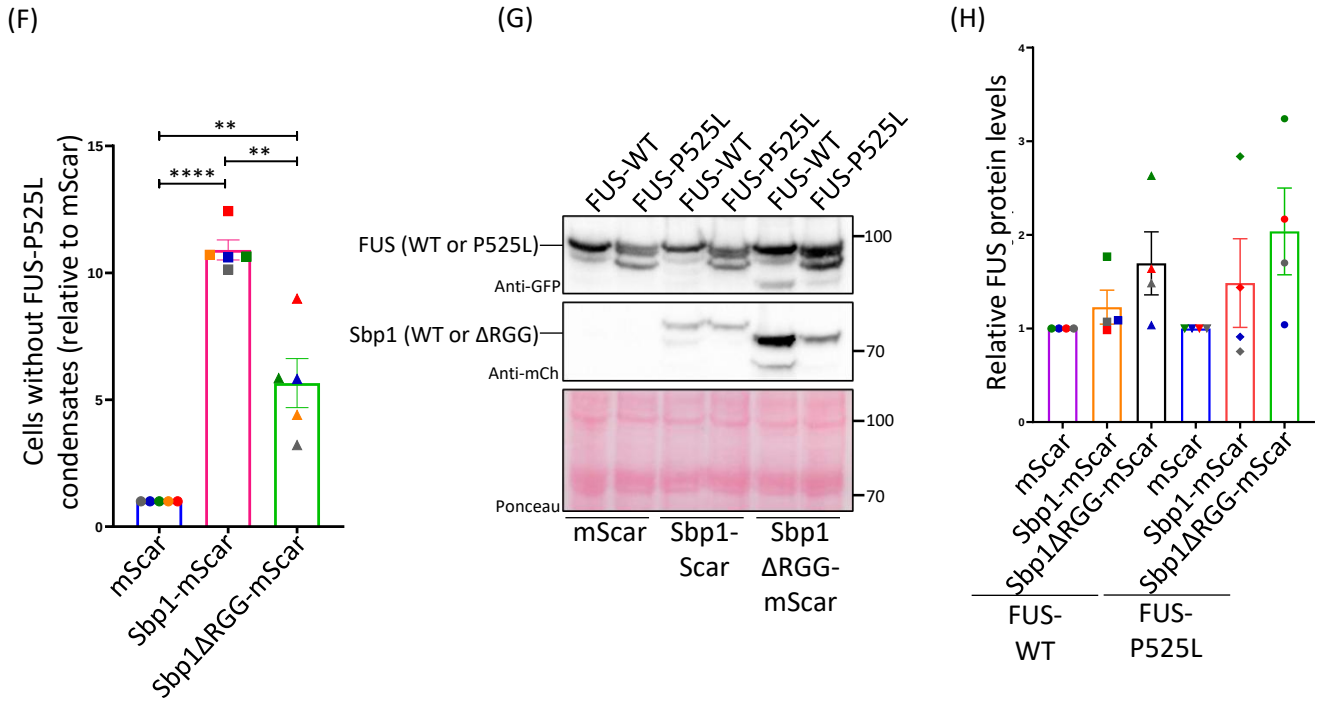

Figure 2: Sbp1 expression reduces mutant TDP43 and FUS condensates in an RGG-motif-dependent manner in mammalian cells. (A) Microscopy images of HEK293T cells co-transfected with mScar/Sbp1-mScar/Sbp1ΔRGG-mScar and different eGFP-TDP43-related constructs. Cells were collected 24 hours after transfection and processed for microscopy analysis. The white arrow marks the presence of cytoplasmic condensates. Scale bar=5um. (B) Graph representing the relative changes in the cells without TDP43-ΔNLS condensates (relative to the mScar transfected cells). The values were also normalized with the respective mScarlet fluorescent intensity expression levels. A paired t-test was used to calculate the significance value (n=6). (C and D) Western blot analysis (C) and its quantitation (D) representing the change in the levels of TDP43-WT and TDP43-ΔNLS in the presence of mScar/Sbp1-mScar/Sbp1ΔRGG-mScar from 6 independent experiments (n=6). Anti-mCh antibody was used to detect the mScarlet-tagged proteins. Values on the right represent the position of different molecular weight ladder bands in kDa. A student-paired t-test was used to calculate the significance value. (E) Microscopy images of HEK293T cells co-transfected with mScar/Sbp1-mScar/Sbp1ΔRGG-mScar and eGFP-FUS-WT/P525L constructs. Cells were processed similarly to the experiment in A. The white arrow marks the presence of cytoplasmic condensates. Scale bar=5um. (F) Graph representing the relative changes in the cells without TDP43-ΔNLS condensates (relative to the mScar transfected cells). The values were also normalized with the respective mScarlet fluorescent intensity expression levels. A paired t-test was used to calculate the significance value (n=5). (G and H) Western blot analysis (G) and its quantitation (H) representing the change in the levels of FUS-WT and FUS-P525L in the presence of mScar/Sbp1-mScar/Sbp1ΔRGG-mScar (n=4). Anti-mCh antibody was used to detect the mScarlet-tagged proteins. Values on the right represent the position of different molecular weight ladder bands in kDa. A student-paired t-test was used to calculate the significance value. Error bars in all graphs represent mean ±SEM, and the same color points in a graph depict the data from a single experimental set. *, **, ***, and **** denote p-value≤0.05, ≤0.01, ≤0.001, and ≤0.0001, respectively.

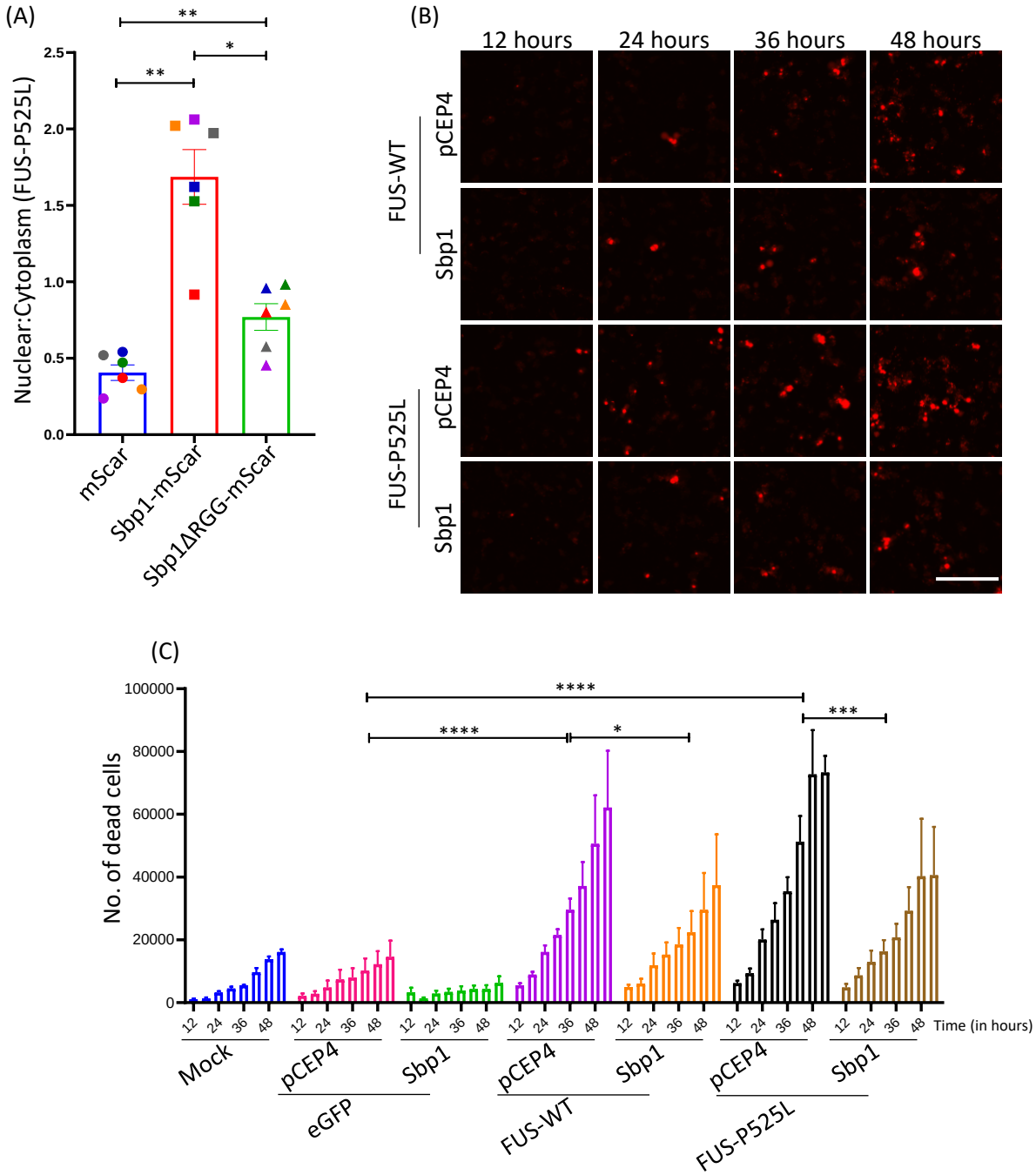

Figure 3: Sbp1 expression reduces overexpression-mediated defects of FUS-P525L in mammalian cells. (A) Graph representing the distribution of FUS-P525L protein in nucleus and cytoplasm. The fluorescent intensities of the nucleus and cytoplasm were calculated from the experiment as performed in Figure 2E, and the ratio is plotted here. A student-paired t-test was used to calculate the significance value (n=6). (B) Incucyte images (real-time cell death analysis) representing the cellular uptake of propidium iodide (PI) in different conditions in HeLa cells. Scale bar=100um. (C) Graph representing the number of propidium iodide (PI) positive cells (dead cells) from the experiment as performed in B. The time on the x-axis reflects the time-point after transfection in hours. The significance was calculated using 2-way ANOVA with multiple comparisons (n=4). Error bars in all graphs represent mean ±SEM, and the same color points in A depict the data from a single experimental set. *, **, ***, and **** denote p-value≤0.05, ≤0.01, ≤0.001, and ≤0.0001, respectively.

Figure 4

(A) *In-cell* sedimentation assay

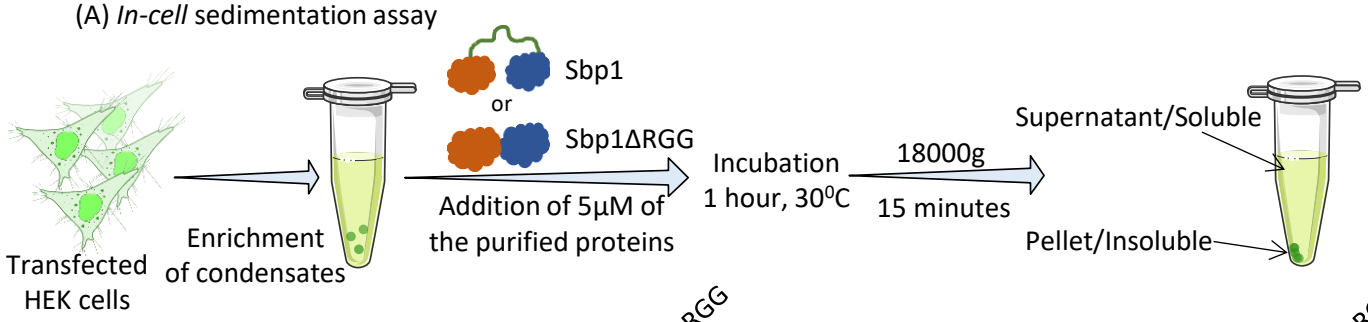

(B)

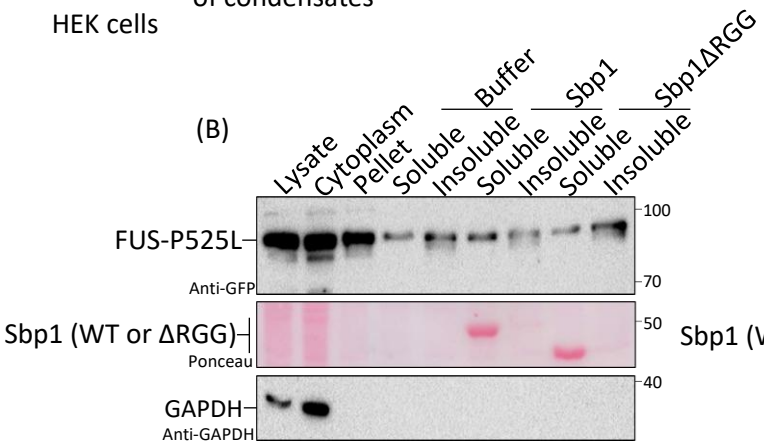

(D)

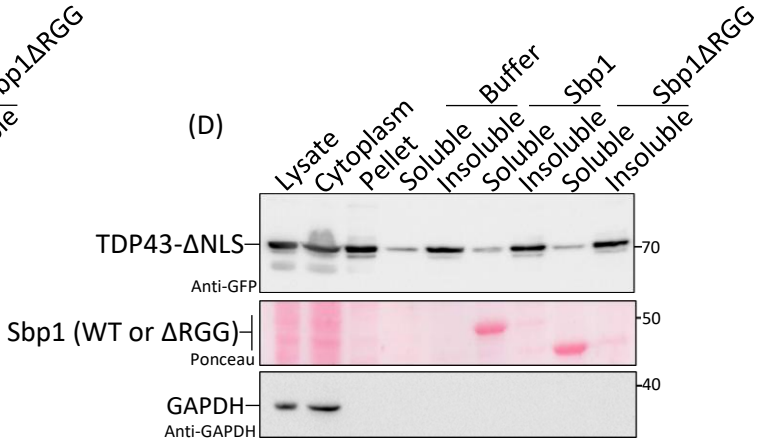

(C)

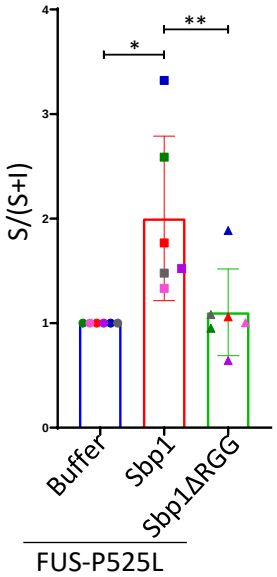

(E)

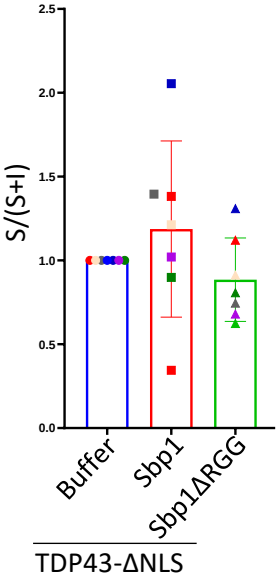

(F) *In-vitro* sedimentation assay

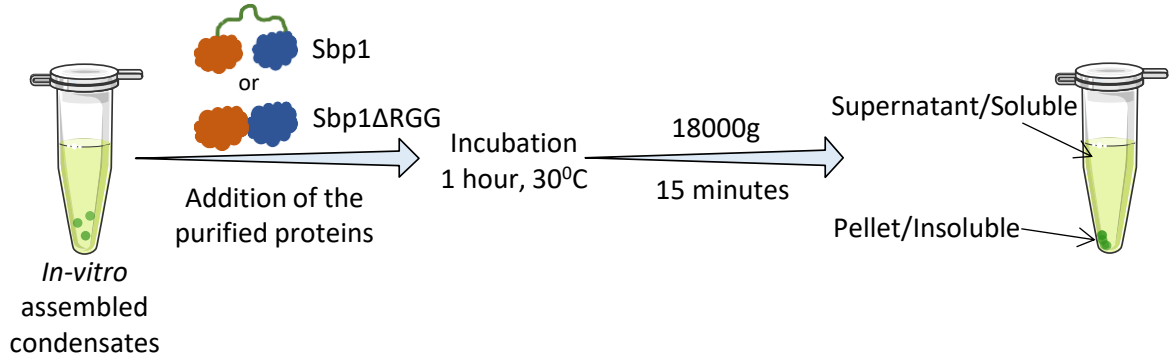

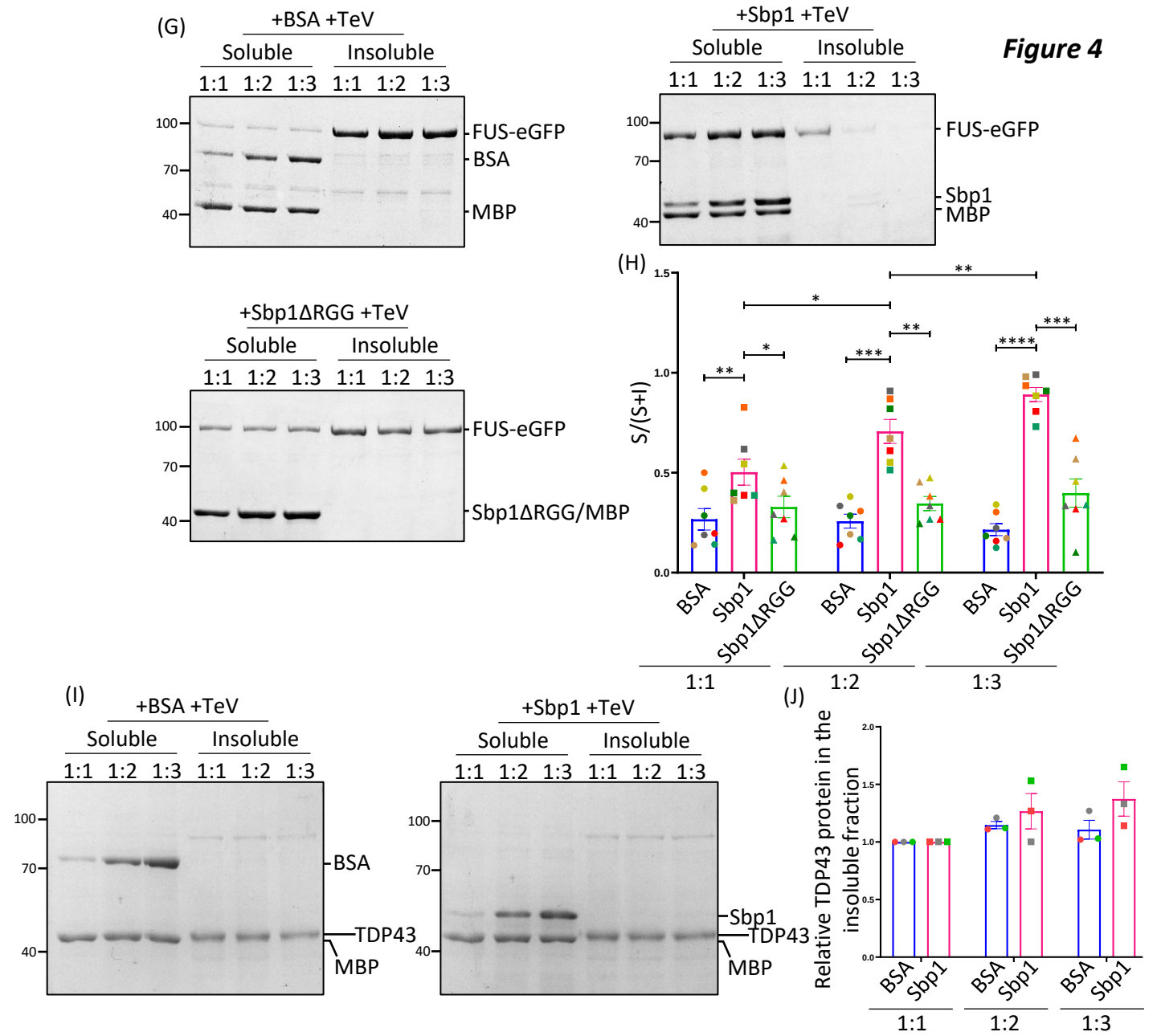

Figure 4: Sbp1, but not Sbp1ΔRGG, disassembles FUS condensates. (A) Schematic depicting the workflow for the *in-cell* sedimentation assay modified to assess the disassembly activity of Sbp1. (B and D) Western analysis of the different fractions from FUS-P525L (B), and TDP43-ΔNLS (D) *in-cell* sedimentation assay. The different fraction loadings are as follows: lysate: 7.5%, cytoplasm: 7.5%, pellet: 15%, soluble: 60%, and insoluble: 60%. GAPDH serves as the control for the assay, and ponceau reflects the purified protein added to the respective reaction. Values on the right represent the position of different molecular weight ladder bands in kDa. (C and E) Quantitation of the amount of protein in the soluble fraction from experiments as done in B and D. The band intensities were calculated using ImageJ, and the fraction of protein in the soluble phase was calculated by S/(S+I), where S and I represent the protein in the soluble and the insoluble fractions, respectively. Significance was calculated by using student-paired t-test analysis (n=6 and n=7 for C and E, respectively). (F) Schematic depicting the workflow of the *in-vitro* sedimentation assay performed to assess the disassembly activity of Sbp1 on the phase-separated FUS and TDP43 condensates. (G) Coomassie-stained protein gels depicting the fractionation of FUS to soluble and insoluble phases in the presence of buffer, BSA, Sbp1, Sbp1ΔRGG. The ratio reflects the amount of FUS: test protein taken for the assay. Sbp1ΔRGG and MBP migrate at the same position and hence appear as a single band. Values on the left represent the position of different molecular weight ladder bands in kDa. (H) Quantitation of the fraction of FUS protein present in the soluble phase from 7 independent experiments (n=7) as performed in G. Significance was calculated by a student-paired t-test analysis. (I) Coomassie-stained protein gels and its quantitation (J) depicting the fractionation of TDP43 to soluble and insoluble phases in the presence of BSA and Sbp1. The ratio reflects the amount of TDP43:test protein taken for the assay. The values on the graph reflect the relative amount of TDP43 protein present in the insoluble fraction. A student-paired t-test analysis calculated significance (n=3). Error bars represent mean ±SEM, and the same color points depict the data from a single experimental set. *, **, ***, and **** denote p-value ≤0.05, ≤0.01, ≤0.001, and ≤0.0001, respectively.

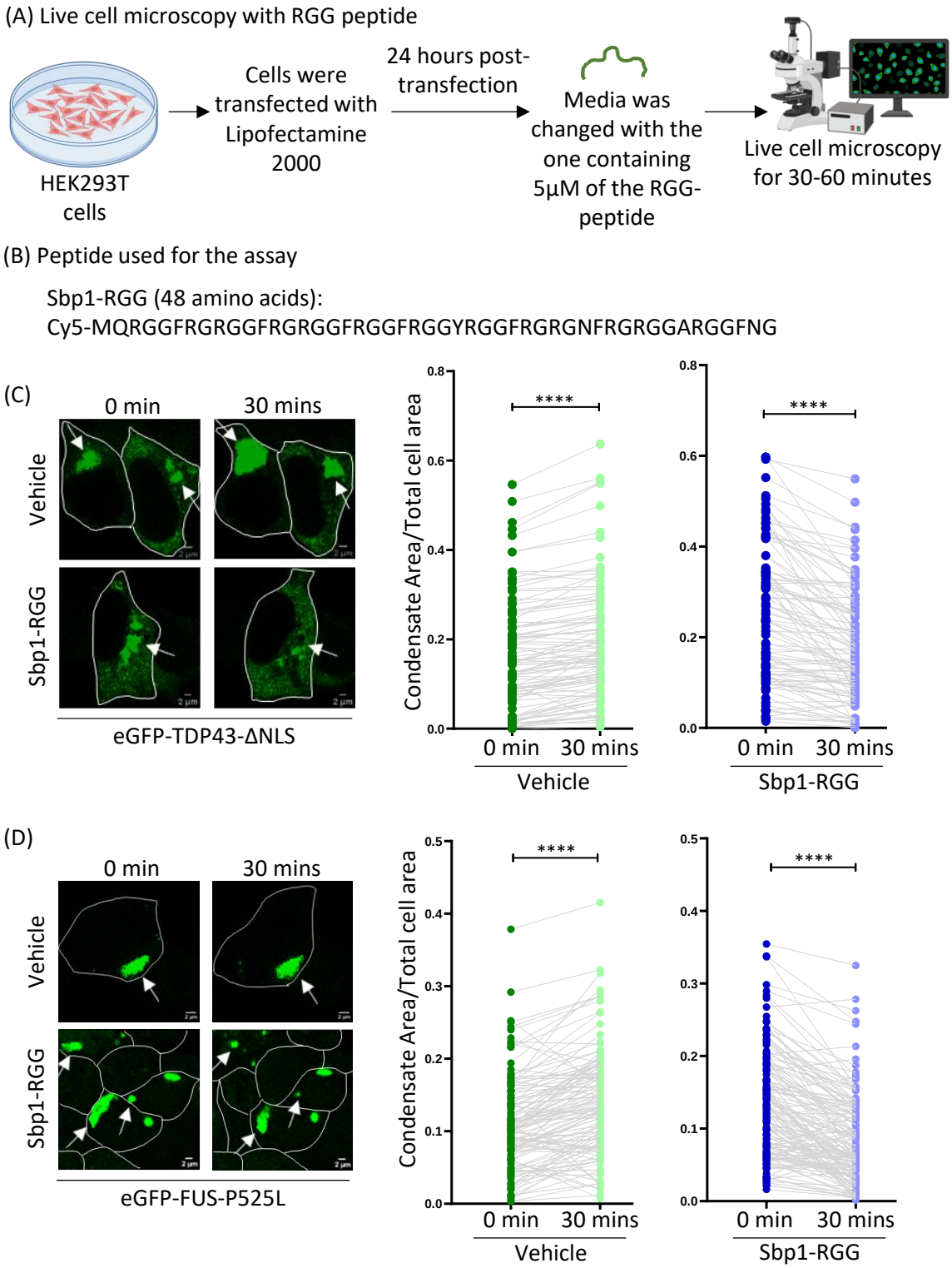

Figure 5: Sbp1-RGG peptide disassembles the TDP43-ΔNLS and FUS-P525L condensates. (A) Schematic depicting the workflow of the live-cell microscopy with the RGG-peptides. (B) The sequence of the peptide used for the experiment as performed in A. 2 extra amino acids at the N-terminal end (M and Q) and 3 amino acids at the C-terminal end (F, N, and G) were included for better purification of the RGG-peptide. (C) Microscopy images for HEK293T cells depicting the change in the area of TDP43-ΔNLS condensate (marked by white arrows) after incubating with either the vehicle control or Sbp1-RGG peptides. Scale bar=2um. Graphs on the right depict the quantitation of the condensate area/total cell area from at least 30 cells per experiment (n=3). (D) Microscopy images for HEK293T cells depicting the change in the area of FUS-P525L condensate (marked by white arrows) after incubating with either the vehicle control or Sbp1-RGG peptides. Scale bar=2um. Graphs on the right depict the quantitation of the condensate area/total cell area from at least 40 cells per experiment (n=3). Significance was calculated by paired t-test analysis. **** denotes p-value $\leq$0.0001.

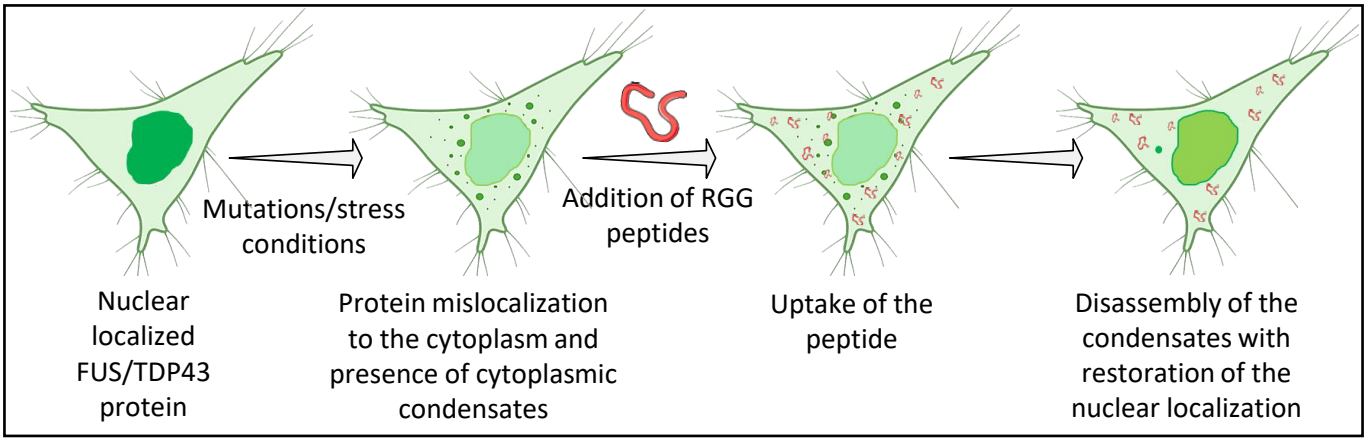

Figure 6: Schematic depicting the role of RGG peptides as a therapeutic approach to disassemble the toxic cytoplasmic condensates. Green represents mutant proteins, like FUS-P525L and TDP43-ΔNLS, that mislocalize to the cytoplasm and form condensates in diseased conditions. RGG peptides could have the potential to disassemble these toxic condensates. Such an effect may also result in the restoration of the nuclear localization phenotype.

Supplementary Figures
S1-S5

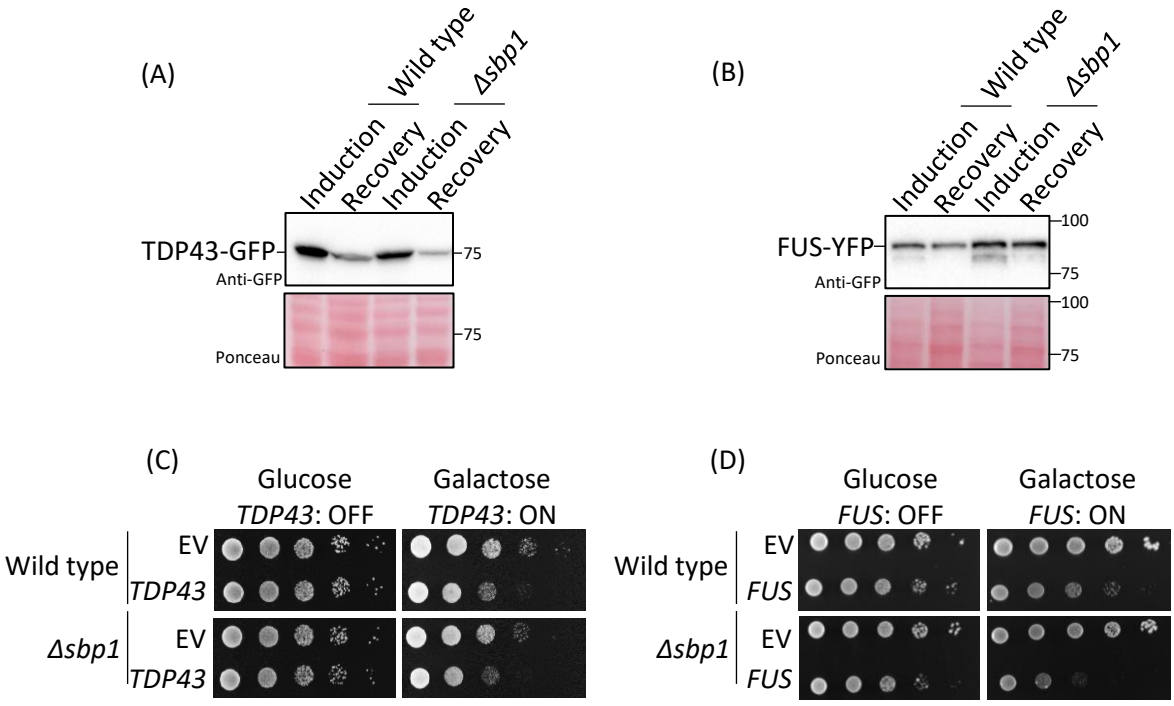

Supplementary Figure S1: Δsbp1 cells are defective in the disassembly of TDP43 and FUS condensates in yeast. (A and B) Western analysis depicting the change in protein levels of TDP43 (A) and FUS (B) with respect to the respective induction condition. Quantitation of the blots is provided as Figure 1D and G. Values on the right represent the position of different molecular weight ladder bands in kDa. Ponceau served as the loading control. (C and D) Spot assays of wild type and Δ*sbp1* cells transformed with either empty vector (EV) or Gal-*TDP43-GFP* (C) / Gal-*FUS-YFP* (D) expressing constructs. After growing to 0.4 OD_{600}, cells were shifted to galactose-containing media for 2-3 hours to induce TDP43/*FUS* expression. This was followed by serial dilution of cells and spotting on glucose and galactose-containing SD-Ura^- media plates. Images were taken after 2 -4 days of growth at 30^0C.

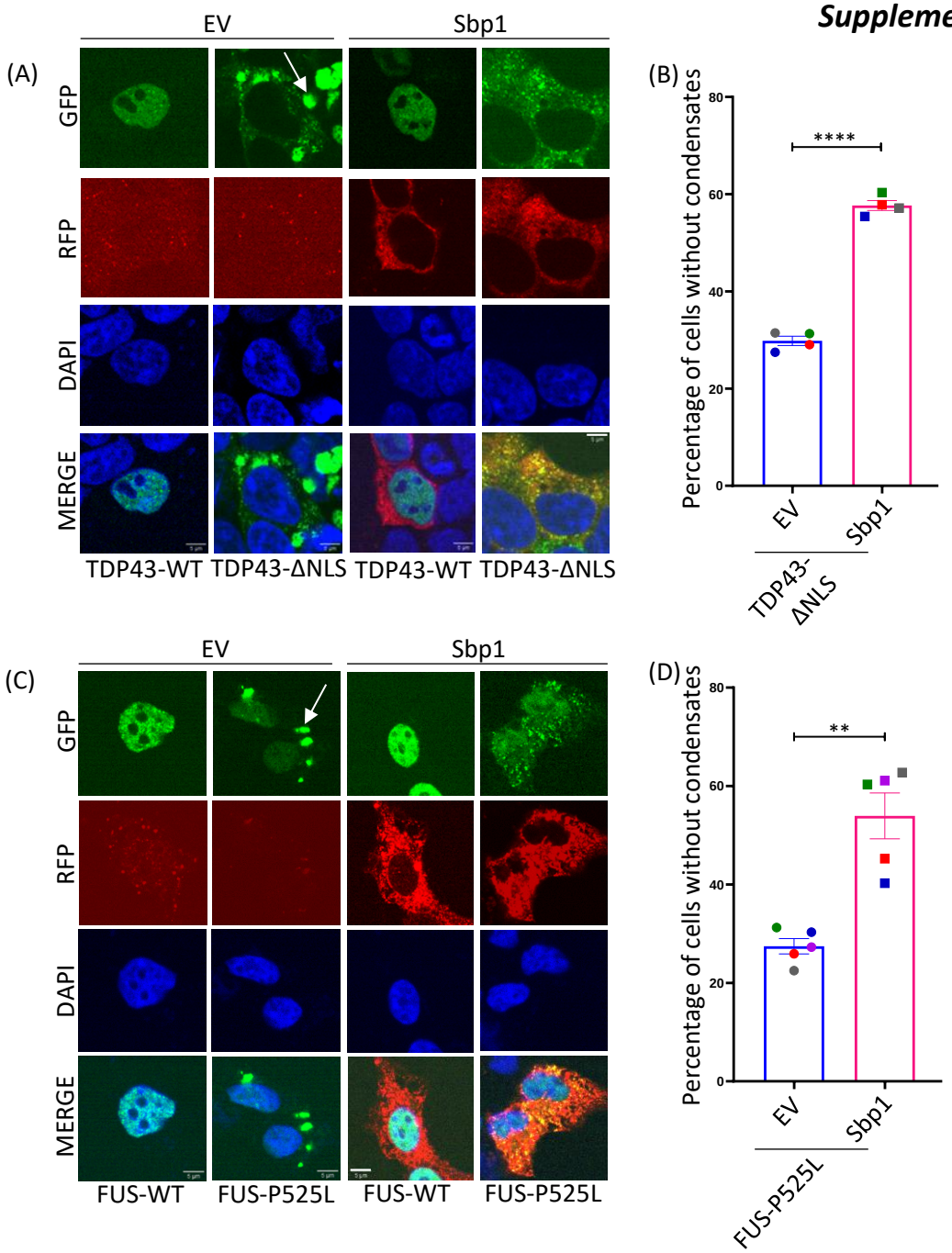

Supplementary Figure S2: Sbp1 expression reduces mutant TDP43 and FUS condensates in HEK293T cells. (A) Microscopy images of HEK293T cells co-transfected with EV/Sbp1 and different eGFP-TDP43-related constructs. Cells were collected 24 hours after transfection and processed for immuno-cytochemistry analysis to detect Sbp1 using an anti-Sbp1 antibody (RFP channel)**.** TDP43 constructs have an N-terminal eGFP-tag that was used to check the localization through the GFP channel. The white arrow marks the presence of cytoplasmic condensates. Scale bar=5um. (B) Quantitation of the percentage of cells without cytoplasmic condensates from the experiment as performed in A. A student-paired t-test was used to calculate the significance value (n=4). (C) Microscopy images of HEK293T cells co-transfected with EV/Sbp1 and eGFP-FUS-WT/P525L constructs. Cells were collected 24 hours after transfection and processed like the experiment in A. The white arrow marks the presence of cytoplasmic condensates. Scale bar=5um. (D) Quantitation of the percentage of cells without cytoplasmic condensates from the experiment as performed in C. A student-paired t-test was used to calculate the significance value (n=5). Error bars in all the graphs represent mean ±SEM, and the same color points in a graph depict the data from a single experimental set. ** and **** denote p-value ≤0.01 and ≤0.0001, respectively.

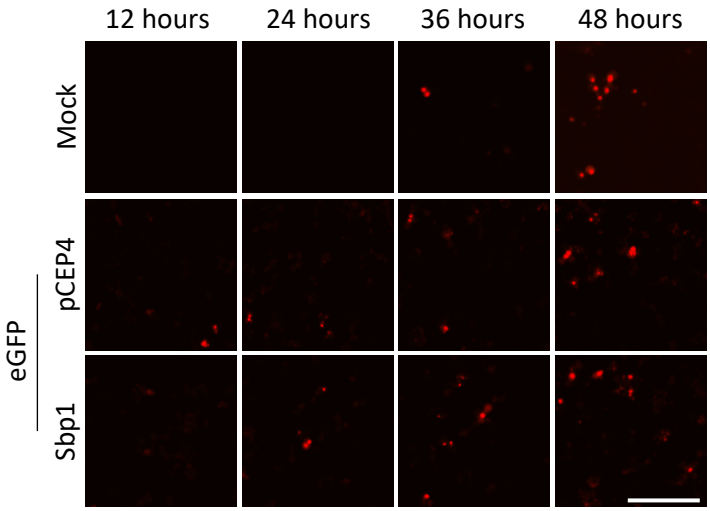

Supplementary Figure S3: Sbp1 expression reduces overexpression-mediated defects of FUS-P525L in mammalian cells. Incucyte images representing the cellular uptake of propidium iodide (PI) in different conditions in HeLa cells. Scale bar=100um. The images are part of Figures 3B and C.

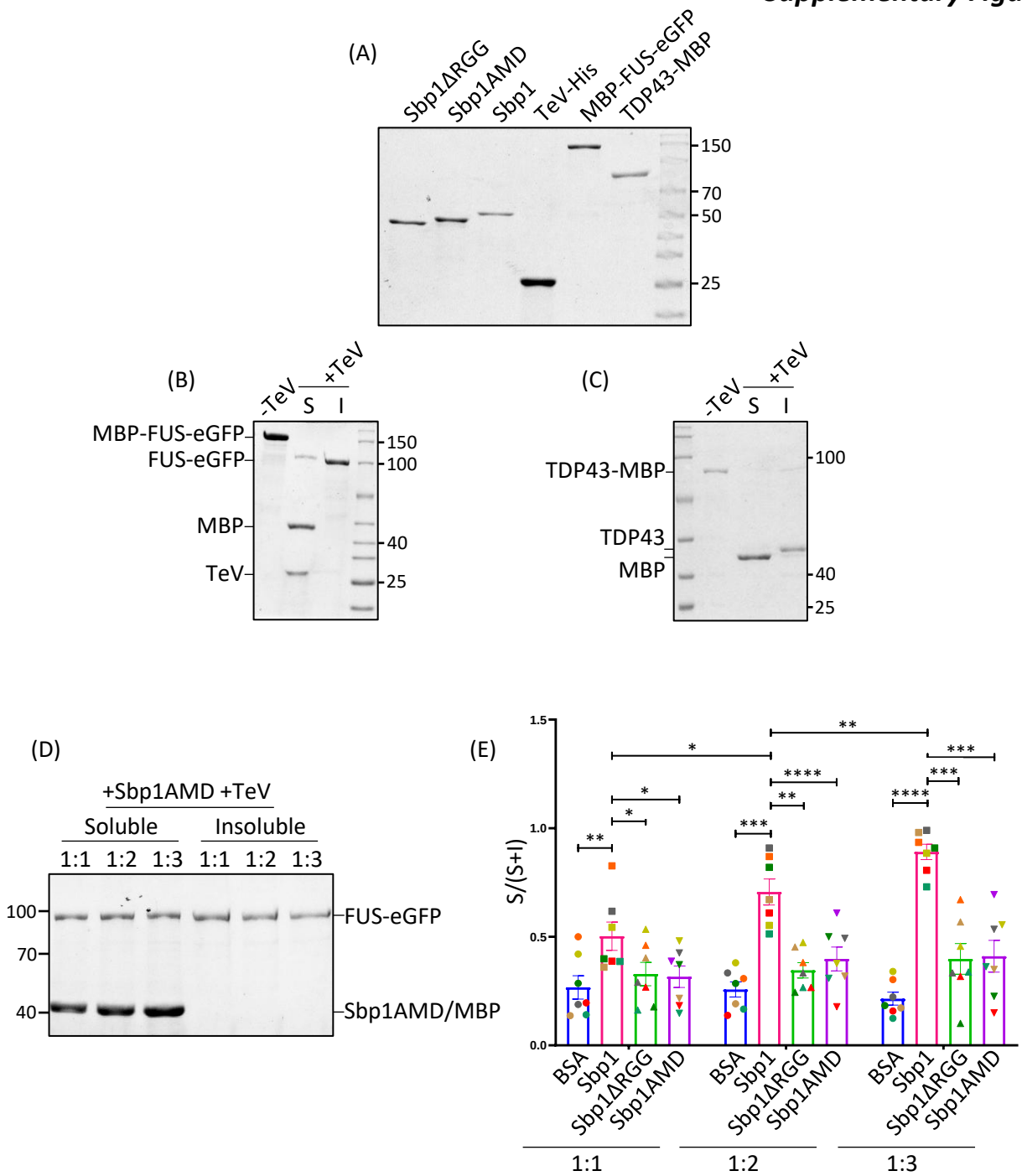

Supplementary Figure S4: Sbp1AMD (arginine methylation defective) mutant does not affect FUS condensates. (A) Coomassie-stained protein gel depicting the various purified proteins used in this study. (B and C) Coomassie-stained protein gels depicting the partitioning of FUS (B) and TDP43 (C) to the insoluble (I) phase after the cleavage of MBP-tag using TeV protease. S denotes the soluble phase. Values on the right represent the position of different molecular weight ladder bands in kDa. (D) Coomassie-stained protein gel depicting the fractionation of FUS to soluble and insoluble phases in the presence of Sbp1AMD (mutant where all arginines within the RGG-motif are covered to alanine, see Figure 1A). The ratio reflects the amount of FUS: test protein taken for the assay. Sbp1AMD and MBP migrate at the same position and hence appear as a single band. Values on the left represent the position of different molecular weight ladder bands in kDa. (E) Quantitation of the fraction of FUS protein present in the soluble phase from 7 independent experiments (n=7) as performed in D and Figure 3H. The graph from Figure 3I has been replotted here to include Sbp1AMD values. Error bars represent mean ±SEM, and the same color points in a graph depict the data from a single experimental set. *, **, ***, and **** denote p-value ≤0.05, ≤0.01, ≤0.001, and ≤0.0001, respectively.

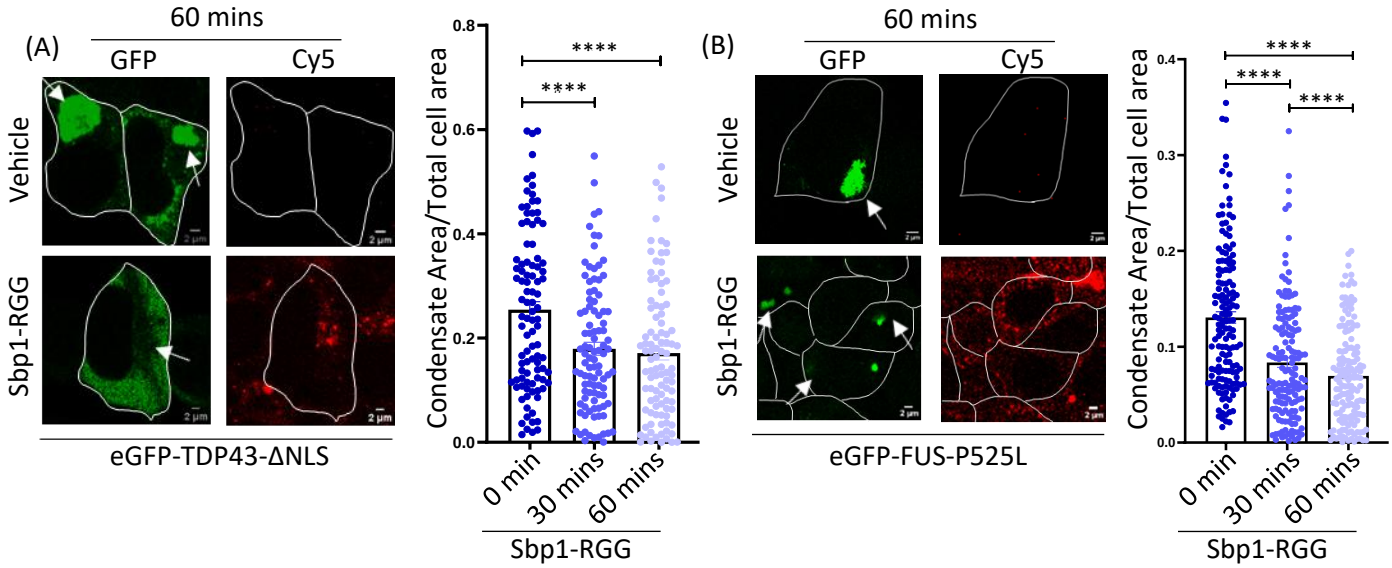

Supplementary Figure S5: HEK293T cells readily uptake Cy5-labelled Sbp1-RGG peptide. (A and B) Microscopy images for HEK293T cells depicting the change in the area of TDP43-ΔNLS (A) and FUS-P525L (B) condensate (marked by white arrows) and the uptake of Cy5-labelled peptide after 60mins of incubation with either the vehicle control or Sbp1-RGG peptides. The panel represents the same set of cells as depicted in Figure 4D. Cy5 panel depicts the uptake of the peptide. Scale bar=2um. The graph on the right represents the change in the condensate area normalized with the total cell area after incubation with the Sbp1-RGG peptide (n=3). The data plotted is the same as Figure 4D with the addition of a 60 mins time point. Error bars represent mean ±SEM. Significance was calculated by paired t-test analysis. **** denotes p-value ≤0.0001.